Bioorganic Chemistry 87 (2019) 572–584

Contents lists available at ScienceDirect

Bioorganic Chemistry

journal homepage: www.elsevier.com/locate/bioorg

Multi-target-directed triazole derivatives as promising agents for the treatment of Alzheimer's disease

Anupamjeet Kaur[a], Sukhmani Mann[a], Amandeep Kaur[a], Nitesh Priyadarshi[c], Bhupesh Goyal[b,*], Nitin Kumar Singhal[c,*], Deepti Goyal[a,*]

[a] Department of Chemistry, Faculty of Basic and Applied Sciences, Sri Guru Granth Sahib World University, Fatehgarh Sahib 140406, Punjab, India
[b] School of Chemistry and Biochemistry, Thapar Institute of Engineering & Technology, Patiala 147004, Punjab, India
[c] National Agri-Food Biotechnology Institute, S.A.S. Nagar, Punjab, India

ARTICLE INFO

Keywords:
Alzheimer disease
Multifunctional inhibitor
Amyloid-β (Aβ) aggregation
Reactive oxygen species
Metal chelator
Triazole-based compound

ABSTRACT

A novel series of triazole-based compounds have been designed, synthesised and evaluated as multi-target-directed ligands (MTDLs) against Alzheimer disease (AD). The triazole-based compounds have been designed to target four major AD hallmarks that include Aβ aggregation, metal-induced Aβ aggregation, metal dys-homeostasis and oxidative stress. Among the synthesised compounds, **6n** having *o*-CF_3 group on the phenyl ring displayed most potent inhibitory activity (96.89% inhibition, IC_{50} = 8.065 ± 0.129 μM) against $A\beta_{42}$ aggregation, compared to the reference compound curcumin (95.14% inhibition, IC_{50} = 6.385 ± 0.009 μM). Compound **6n** disassembled preformed $A\beta_{42}$ aggregates as effectively as curcumin. Furthermore, **6n** displayed metal chelating ability and significantly inhibited Cu^{2+}-induced $A\beta_{42}$ aggregation and disassembled preformed Cu^{2+}-induced $A\beta_{42}$ aggregates. **6n** successfully controlled the generation of the reactive oxygen species (ROS) by preventing the copper redox cycle. In addition, **6n** did not display cytotoxicity and was able to inhibit toxicity induced by $A\beta_{42}$ aggregates in SH-SY5Y cells. The preferred binding regions and key interactions of **6n** with $A\beta_{42}$ monomer and $A\beta_{42}$ protofibril structure was evaluated with molecular docking. Compound **6n** binds preferably to the C-terminal region of $A\beta_{42}$ that play a critical role in $A\beta_{42}$ aggregation. The results of the present study highlight a novel triazole-based compound, **6n**, as a promising MTDL against AD.

1. Introduction

The highly ordered peptide or protein aggregates in brain are thought to be responsible for a number of protein misfolding diseases in humans that include Alzheimer disease (AD), Parkinson disease, Creutzfeldt-Jakob disease, type II diabetes, *etc.* AD is the most common form of dementia, with no treatment available to completely cure or halt its progression. The characteristic symptoms of AD are progressive memory loss, cognitive impairment, and behaviour changes like depression, aggression, *etc.* [1]. Around 50 million people are affected with dementia worldwide and the number will reach to 152 million by 2050 [2]. The precise molecular mechanism behind the pathogenesis of AD remains elusive. A number of hypotheses have been proposed for the pathomechanism of AD that include *β*-amyloid deposits, abnormally phosphorylated and *β*-folded tau protein, metal ion dyshomeostasis and oxidative stress that highlight the multifactorial nature of AD [3]. The FDA approved drugs (rivastigmine [4], donepezil [5], galantamine [6] and memantine [7]) for AD target neurotransmitter abnormalities associated with the disease and do not affect the underlying etiology. These drugs at best provide only temporary and incomplete symptomatic relief [8]. Moreover, the recent failure of various moieties such as PPI-1019 [9], NAP (NAPVSIPQ) [10], tarenflurbil [11], semagacestat

Abbreviations: Aβ, Amyloid-β; Ac, Acetyl; Ac_2O, Acetic anhydride; AD, Alzheimer's disease; APP, Amyloid precursor protein; ANOVA, Analysis of variance; CCA, Coumarin-3-carboxylic acid; CQ, Clioquinol; DCM, Dichloromethane; DMEM, Dulbecco's modified eagle's medium; DMSO, Dimethyl sulfoxide; Et, Ethyl; EtOH, Ethanol; HEPES, 4-(2-Hydroxyethyl)-1-piperazineethanesulfonic acid; HF, Hatree-Fock; HFIP, 1,1,1,3,3,3-Hexafluoro-2-propanol; HRMS, High resolution mass spectrometry; LRMS, Low resolution mass spectrometry; MTDLs, Multi-target-directed ligands; MTT, 3-(4,5-Dimethylthiazol-2-yl)-2,5-diphenyltetrazolium bromide; NMR, Nuclear magnetic resonance; PBS, Phosphate-buffered saline; PDB, Protein data bank; RMSD, Root mean square deviation; ROS, Reactive oxygen species; TBAHS, Tetrabutylammonium hydrogen sulfate; TEM, Transmission electron microscopy; *t*-BuOH, *tert*-Butyl alcohol; ThT, Thioflavin-T; TLC, Thin layer chromatography; UV-Vis, Ultraviolet-visible

* Corresponding authors.
E-mail addresses: bhupesh@iitbombay.org (B. Goyal), nitin@nabi.res.in (N.K. Singhal), deeptig@iitbombay.org (D. Goyal).

https://doi.org/10.1016/j.bioorg.2019.03.058
Received 6 October 2018; Received in revised form 6 March 2019; Accepted 19 March 2019
Available online 23 March 2019

[12], avagacestat [13], LY2886721 [14], bapineuzumab [15], solanezumab [16], PBT1 and PBT2 [17] in clinical trials highlight the urgent need to identify and develop new molecules as future drug candidates for AD. Considering the complex pathomechanism of AD, future developments of AD modifying therapies need to take into account the new "multi-target-directed ligands" (MTDLs) paradigm [18].

A large number of studies highlighted that amyloid plaques as well as soluble oligomers formed by the deposition of amyloid-β (Aβ) peptide (39–43 amino acid residues) play a critical role in the pathophysiology of AD [19]. Aβ results from the proteolytic cleavage of the amyloid precursor protein (APP) by enzymes *α*-secretase, *β*-secretase and γ-secretase [20]. The Aβ oligomers interact with neurons and glial cells that result in the activation of pro-inflammatory cascades, and finally cause neuronal apoptosis and cell death. Thus, designing anti-aggregation agents that inhibit the self-assembly of Aβ peptide and destabilize the protofibril structure will provide a potent therapeutics against AD [21].

The recent studies highlighted that dysregulation of brain metal ion (copper and zinc) homeostasis, play a critical role in the pathogenesis of AD [22]. The amyloid plaques are found to be enriched with Cu^{2+} and Zn^{2+}. These metal ions are found to coordinate with histidine residues in senile plaque core, which results in the accumulation of the metal ions in the extracellular plaques. As a result, the intracellular copper stores become deficient in AD patient. This promotes a vicious cycle of metal ion accumulation and plaque formation [23]. Thus, modulating the concentration of these biometals has been highlighted as a possible therapeutic strategy for AD, and various metal chelators have been proposed in literature [24]. Moreover, studies highlighted that inappropriate accumulation of redox-active metal ions (Cu and Fe) cause oxidative stress that ultimately lead to neuronal cell death by the generation of reactive oxygen species (ROS) through Haber-Weiss and Fenton-like reactions [25]. Thus, designing MTDLs that can inhibit Aβ aggregation, metal-induced Aβ aggregation and reduce oxidative stress provide an effective approach for the treatment of AD [26].

In this regard, a library of di-triazole based compounds **6(a-p)** was designed, synthesised and evaluated as promising drug candidates against AD in the present study. The nitrogen containing heterocyclic rings with diverse biological activities [27] provide a viable starting point for the design of new molecular entities for AD treatment. Notably, these ring systems have been explored in designing effective drug candidates and scanning probes in various neurodegenerative diseases. Qu et al. reported radiolabeled diphenyltriazole derivatives as imaging agents for targeting Aβ plaques [28]. In 2017, Smid and co-workers highlighted that the triazole acetamide scaffold as an effective aggregation inhibitor against AD [29]. Vajragupta and co-workers reported three series of substituted anti-1,2,3-triazoles (IND, PPRD, and QND) as α7 nicotinic acetylcholine receptor agonists [30]. Jones et al. synthesised 1,2,3-triazole derivatives (POH, PMorph, PTMorph) and highlighted that triazole derivatives inhibit Aβ aggregation as well as metal induced Aβ aggregation, and display metal chelation and antioxidant activity [31]. Jiaranaikulwanitch et al. reported tryptoline and tryptamine triazole derivatives as multifunctional ligands for the treatment of AD [32]. In the present study, a series of di-triazole based compounds **6(a-p)** are reported as MTDLs against AD that possess anti-$A\beta_{42}$ aggregation, inhibition of metal-induced $A\beta_{42}$ aggregation, disaggregation of preformed $A\beta_{42}$ fibrils, metal chelation, and radical scavenging properties.

2. Results and discussion

2.1. Rational design of MTDLs

The rationale to design a drug candidate for targeting the multifactorial disease such as AD, is based on the polypharmacology concept [33]. The designed pharmacophore model comprised of two parts: hydrophobic part and the metal chelator part (Fig. 1). The hydrophobic part consists of phenyl group, which helps to induce the hydrophobic contacts between the ligand and Aβ peptide to disrupt peptide-peptide interaction and produce an anti-aggregation effect. The metal chelator part, containing di-triazole moiety, has the property to chelate metal ions [34] and are able to modulate $A\beta_{42}$ aggregation in the presence of copper. The metal chelating property of the designed triazole based compounds helps to reduce the oxidative stress by disrupting the copper-ascorbate redox system. The designed di-triazole based compounds are assembled by highly regioselectivity copper catalysed Huisgen cycloaddition reaction [35]. Further, the synthetic strategy and structural variance assimilated by Huisgen cycloaddition reaction, highlights the influence of R-group variation on the ligand-$A\beta_{42}$ interactions.

The target compounds **6(a-p)** were assembled according to the synthetic sequence depicted in Scheme 1. The designed di-triazole based compounds **6(a-p)** were synthesised *via* Huisgen cycloaddition reaction between di-alkyne **4** and azides **5(a-p).** To realize the designed strategy, we first assembled the di-alkyne building block **4** in three steps starting from ethyl isocyanoacetate **1** [36]. In this regard, compound **1** was propargylated in the presence of tetrabutylammonium hydrogen sulfate (TBAHS) to furnish the isonitrile derivative **2.** Compound **2** was hydrolysed under acidic conditions to yield the amino ester **3**. The acetylation of the NH_2 group in **3** delivered the desired di-alkyne building block **4**. On the other hand, various azides **5(a-p)** were synthesised from the corresponding amines according to the literature procedure [37]. Finally, the di-alkyne derivative **4** was reacted with differently substituted phenyl azides to yield the designed di-triazole based compounds **6(a-p)** listed in Table 1. The formation of compounds **6(a-p)** were confirmed by complementary spectral data (^{1}H NMR, ^{13}C NMR and HRMS/LRMS).

2.2. Inhibition of self-mediated $A\beta_{42}$ aggregation by synthesised MTDLs

The effect of di-triazole based compounds **6(a-p)** on $A\beta_{42}$ aggregation was examined by performing a thioflavin-T (ThT) fluorescence binding assay. ThT fluorescence can be employed to monitor the formation of $A\beta_{42}$ fibrils as ThT, a cationic benzothiazole dye, undergoes a large augmentation in its fluorescence emission upon binding to amyloid fibrils [38]. The low intensity of ThT fluorescence value indicates the less formation of β-sheet structure. In order to perform the ThT assay, we first optimized the experimental conditions, *i.e.*, concentration of $A\beta_{42}$ and ThT to be used, and time of incubation and consequently the optimized conditions were used in the studies. Curcumin (a known Aβ aggregation inhibitor) was used as reference compound in the present assay [39]. The results shown in Fig. 2A indicate that most of the synthesised compounds display moderate to good potencies compare to curcumin. Among them, compounds **6g-6h**, **6l** and **6n**, exhibited more than 50% inhibition of $A\beta_{42}$ aggregation. Compound **6n** featuring *o*-CF_3 group on the phenyl ring exhibited most potent inhibitory activity against $A\beta_{42}$ aggregation, *i.e.*, 96.89%, better than the reference compound curcumin (95.14%). The complete dose-response curve of compound **6n** was evaluated. The curve shows that compound **6n** inhibited $A\beta_{42}$ aggregation with an IC_{50} value of 8.065 ± 0.129 μM as compare with the control, curcumin (IC_{50} = 6.385 ± 0.009 μM). The ability of **6n** to inhibit self-mediated $A\beta_{42}$ aggregation was further confirmed by transmission electron microscopy (TEM) assay. The incubation of $A\beta_{42}$ at 37 °C for 24 h produced long rope-like amyloid fibrils (Fig. 2Bb) as compared to $A\beta_{42}$ at 0 h (Fig. 2Ba). In contrast, the formation of amyloid fibrils was significantly reduced in the presence of compound **6n** (Fig. 2Bc) under the similar experimental conditions, which highlight that **6n** inhibited $A\beta_{42}$ aggregation. The excellent inhibitory activity of **6n** can be attributed to the presence of strong electron withdrawing –CF_3 group, which increases the occurrence of non-covalent interaction and hydrogen bond formation. The –CF_3 group stabilize the interaction between protein and ligand through charge distribution and stabilize Aβ peptide in the *α*-helix conformation [40].

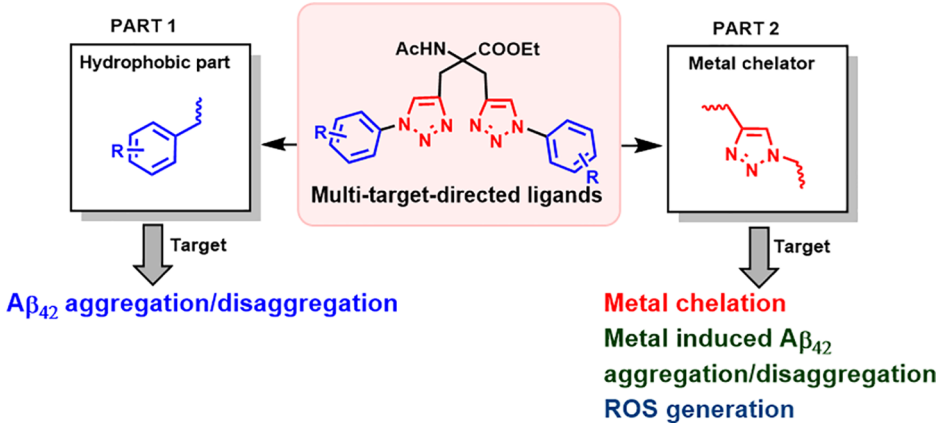

Fig. 1. Rational design of di-triazole based compounds as multifunctional agents for the treatment of AD.

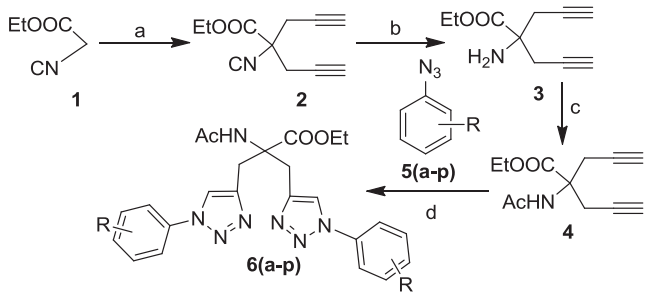

Scheme 1. Synthetic sequences for the synthesis of designed MTDLs **6(a-p)**. Reagents and reaction conditions: (a) Propargyl bromide, K_2CO_3, Tetrabutylammonium hydrogen sulfate (TBAHS), CH_3CN, reflux, 16 h, 92%; (b) EtOH/HCl, rt, 2 h, 91%; (c) Ac_2O, DCM, rt, 3 h, 83%; (d) $Cu(OAc)_2$, Na-ascorbate, *t*-BuOH/H_2O (1:1), rt.

2.3. Effect of compound *6n* on disaggregation of self–mediated $A\beta_{42}$ aggregation fibrils

The disaggregation of preformed $A\beta_{42}$ fibrils by **6n** was investigated using ThT fluorescence assay. The $A\beta_{42}$ fibrils were generated by incubating fresh $A\beta_{42}$ monomer (20 μM) for 24 h at 37 °C. Compound **6n** and curcumin (reference compound) were then added separately to the samples before incubating for another 24 h at 37 °C. The results of the ThT fluorescence assay were shown in Fig. 3A, which indicated that **6n** was as effective as curcumin in disaggregating preformed $A\beta_{42}$ fibrils (**6n**: 81.89% at 40 μM; curcumin: 85.75% at 40 μM). The results of the ThT assay were further complimented by TEM assay. The results indicated that $A\beta_{42}$ alone had aggregated into amyloid fibrils (Fig. 3Bb) after 24 h incubation at 37 °C. The co-incubation of preformed fibrils with **6n** for 24 h significantly reduced the amount of Aβ fibrils as shown in the TEM images (Fig. 3Bc). These results highlighted that **6n** can effectively disassembled the self-mediated $A\beta_{42}$ fibrils.

2.4. Ability of compound *6n* to chelate biometals

The chelating ability of compound **6n** towards biometals such as Cu^{2+}, Zn^{2+}, Fe^{2+} was examined by UV–Vis spectroscopy [26]. The specific absorbance peaks of **6n** were observed at 222 and 262 nm as shown in Fig. 4a. After the addition of Cu^{2+} to the solution of **6n**, there was a dramatic increase in the absorbance at 262 nm, highlighting an interaction between **6n** and Cu^{2+}. When Zn^{2+} was added to the solution of **6n**, a decrease in the absorbance at 222 nm and a slight increase in absorbance at 262 nm was observed. Similarly, the absorbance at 262 nm increases on addition of Fe^{2+} to a solution of **6n**, suggesting that **6n** binds to Zn^{2+} and Fe^{2+}. The metal chelating ability of **6n** could be due to the donation of lone pair of electron on one of the π-bonded nitrogen atoms present in the triazole ring.

In order to determine the binding stoichiometry of **6n** with Cu^{2+}, a series of solutions were prepared according to the Job's method [41]. The total concentration of compound **6n** and $CuSO_4$ remains constant, however, their proportion were varied. The absorbance of complex of $CuSO_4$ and **6n** at different concentrations were recorded on a UV–Vis spectrometer (Fig. S1, Supplementary material). As shown in Fig. 4b, the absorbance at 262 nm increases initially and thereafter decreases, which yield two straight lines that intersect at a mole fraction of 0.3, which in turn highlights a 2:1 stoichiometry for **6n**–Cu^{2+} complex.

2.5. Ability of compound *6n* to suppress copper-based redox activity

Copper play a critical role in the formation of ROS, which lead to an increase in the oxidative stress. The excessive generation of ROS may activate neuronal cell death in AD patients. Thus, compound **6n** was examined for its ability to halt the production of ROS by utilizing the Cu-ascorbate redox system described in Scheme 2, as a model system [42]. The generation of the hydroxyl radicals ($OH^{\cdot}$) during the copper redox cycling were measured by using coumarin-3-carboxylic acid (CCA), which forms fluorescent 7-hydroxy-CCA species (emission at 450 nm). The results in Fig. 5, indicated that $OH^{\cdot}$ produced by copper and ascorbate increases steadily with time and achieved plateau at nearly 12 min. However, this process was completely inhibited in presence of **6n**, highlighting that **6n** has the ability to prevent copper redox cycling involved in the oxidative stress by chelating the metal ions.

2.6. Effect of compound *6n* on Cu^{2+}-mediated $A\beta_{42}$ aggregation

The inhibitory activity of **6n** against $A\beta_{42}$ aggregation in the presence of copper was investigated using ThT fluorescence assay. Fig. 6, clearly indicated that copper accelerates the $A\beta_{42}$ aggregation. According to ThT assay, the percentage of formation of $A\beta_{42}$ fibrils is 42% higher in the presence of Cu^{2+} than $A\beta_{42}$ alone. However, the fluorescence of $A\beta_{42}$ co-incubated with Cu^{2+} and the test compounds decreased notably. The fluorescence after treatment with **6n**, and clioquinol [43] (CQ, a known metal chelator used as reference compound) was 49.01% and 42.25%, respectively. The above results strongly indicate that **6n** was capable of reducing the Cu^{2+} mediated $A\beta_{42}$ aggregation.

2.7. Ability of compound *6n* to disaggregate Cu^{2+}-mediated $A\beta_{42}$ aggregation fibrils

The ability of compound **6n** to disaggregate Cu^{2+}-mediated $A\beta_{42}$ fibrils was studied by ThT fluorescence assay and the results are shown in Fig. 7. The $A\beta_{42}$ fibrils were generated by incubating fresh $A\beta_{42}$ monomer with 1 equiv. of Cu^{2+} for 24 h at 37 °C. Then, **6n** and CQ

Table 1
List of di-triazole derivatives **6(a-p)**.

Cpd	R	Di-triazole derivatives	Yield (%)[a]
6a	H	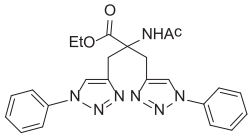	65
6b	*o*-F	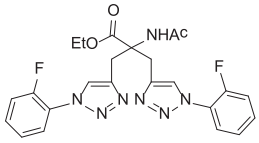	82
6c	*m*-F	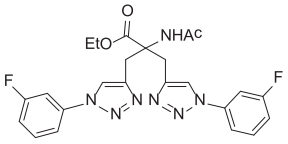	53
6d	*p*-F	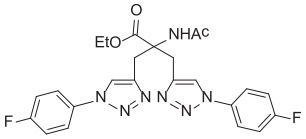	88
6e	*o*-Cl	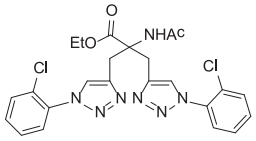	54
6f	*m*-Cl	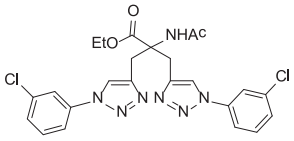	71
6g	*p*-Cl	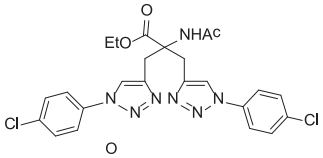	54
6h	*o*-Br	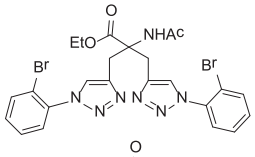	52
6i	*m*-Br	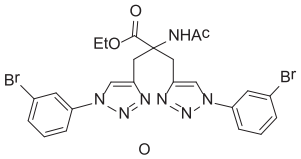	58
6j	*p*-Br	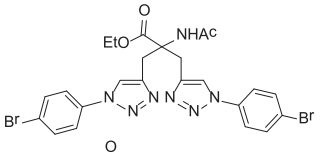	53
6k	*o*-I	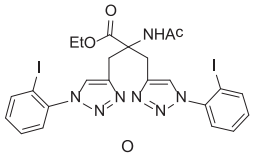	59
6l	*m*-I	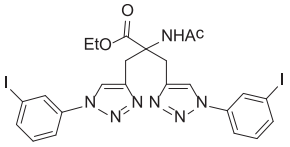	59

Table 1 (*continued*)

Cpd	R	Di-triazole derivatives	Yield (%)[a]
6m	*p*-I	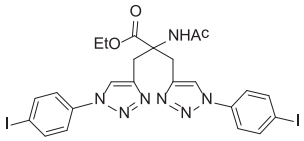	65
6n	*o*-CF_3	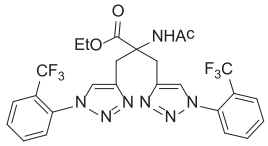	66
6o	*m*-CF_3	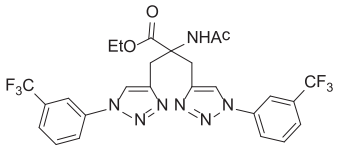	56
6p	*p*-CF_3	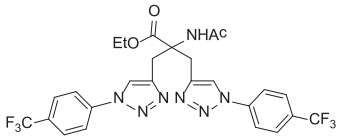	53

[a] Yields were of isolated and purified products.

(40 μM) were added separately to $A\beta_{42}$ fibrils and incubated for another 24 h at 37 °C. The results shown in Fig. 7 indicated that both **6n** and CQ can disaggregate $A\beta_{42}$ fibrils resulting from Cu^{2+}-induced aggregation at 40 μM (**6n**: 61.42%; CQ**:** 65.34% disaggregation).

*2.8. Effect of compound **6n** on neuronal cell viability and on $A\beta_{42}$ mediated neurotoxicity*

3-(4,5-Dimethylthiazol-2-yl)-2,5-diphenyltetrazolium bromide (MTT) reduction assay [44] using SH-SY5Y cells were performed to check the cytotoxicity of compound **6n**. The results shown in Fig. 8a, indicated that the incubation of the SH-SY5Y cells with upto 50 μM concentration of the compound **6n** for 48 h did not influence the cell viability of the stain significantly (cell viability in the presence of **6n**: 97.79% at 5 μM; 95.31% at 25 μM and 90.01% at 50 μM). These results indicated that the compound **6n** is biocompatible.

The $A\beta_{42}$ aggregates were toxic to the SH-SY5Y cells (Fig. 8) and reduced the cell viability to 59% as compared to the control (100%). However, $A\beta_{42}$ co-incubated with **6n** at different molar ratio resulted in higher cell viability. The cell viability increased with increasing the molar ratio of **6n** to $A\beta_{42}$. The cell viability increases to 74.79% at $A\beta_{42}$/**6n** = 1:10. These results suggest that **6n** was able to inhibit the toxicity induced by $A\beta_{42}$ aggregates in SH-SY5Y cells.

*2.9. Molecular docking of **6n** with $A\beta_{42}$ monomer and $A\beta_{42}$ protofibril*

To elucidate the binding regions and key interactions of **6n** with $A\beta_{42}$ monomer, **6n** was docked to $A\beta_{42}$ monomer (PDB ID: 1Z0Q). The negative binding energy (−5.52 kcal/mol, Table 2) highlights the favorable binding between **6n** and $A\beta_{42}$ monomer. A hydrogen bond was observed between the nitrogen atom of triazole ring of **6n** and NH of the backbone of Ala42 of $A\beta_{42}$ (Fig. 9a). **6n** display hydrophobic contacts with Ala30, Ile31, Leu34, Met35, Gly38, Val39, Val40, Ile41, and Ala42 residues of $A\beta_{42}$ monomer (Fig. 10a).

To determine the binding regions of **6n** with $A\beta_{42}$ protofibril, **6n** was docked to $A\beta_{42}$ protofibril (PDB ID: 2BEG). The visualization of

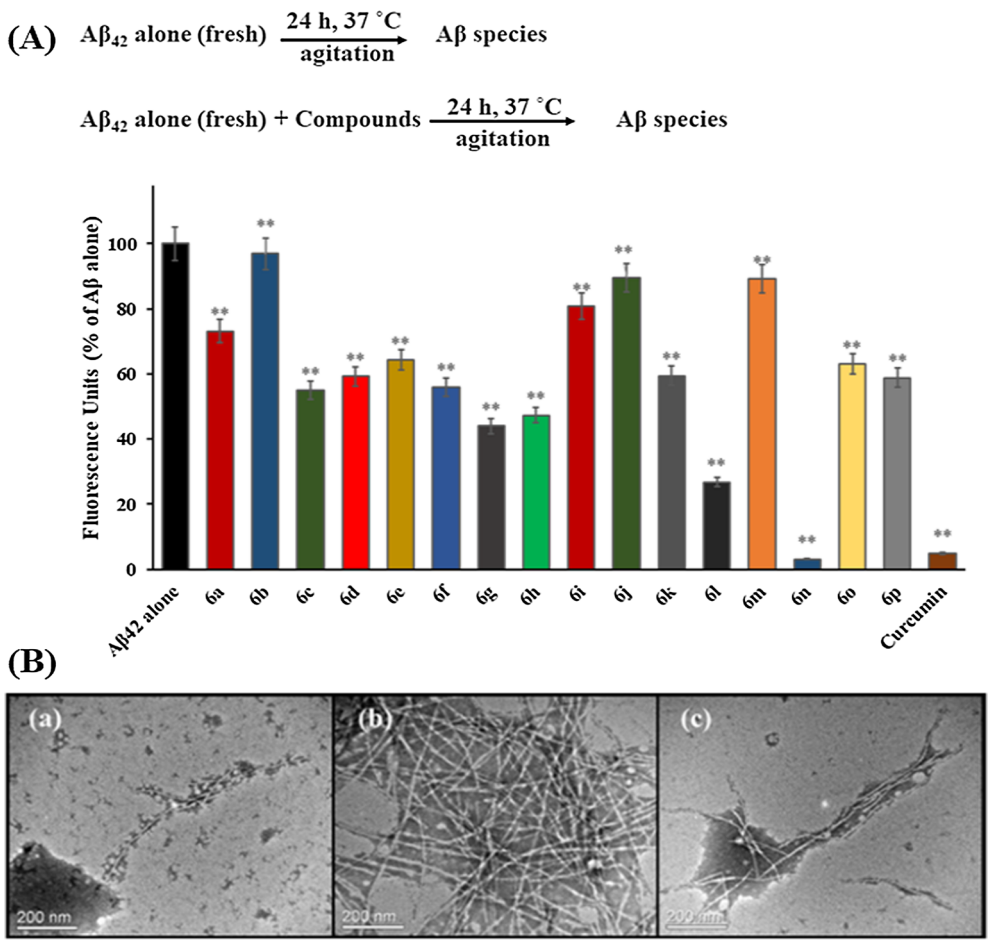

Fig. 2. Inhibition of self-mediated $A\beta_{42}$ aggregation by designed di-triazole based compounds: (A) The results of ThT fluorescence binding assay. The statistical significance was analysed by one-way analysis of variance (ANOVA) followed by Dunnett's test: (**) $p < 0.01$, versus $A\beta_{42}$ alone. $[A\beta_{42}] = 20\ \mu M$, **[6(a-p)]** = [Curcumin] = 100 μM. (B) TEM images of $A\beta_{42}$ aggregation in the presence of compound **6n:** $[A\beta_{42}] = 20\ \mu M$, [**6n**] = 40 μM, 37 °C, 24 h, constant agitation (a) $A\beta_{42}$, 0 h; (b) $A\beta_{42}$, 24 h; (c) $A\beta_{42}$ + **6n**, 24 h. Scale bar: 200 nm.

docked pose highlights that **6n** bind with chain E of $A\beta_{42}$ protofibril and the observed binding energy is −6.75 kcal/mol (Table 2). **6n** form two hydrogen bonds with $A\beta_{42}$ protofibril. The first hydrogen bond was observed between the nitrogen atom of triazole ring of **6n** and NH of the backbone of Ile41(E) of $A\beta_{42}$ protofibril and the second hydrogen bond was formed between the NH of the amide group of **6n** and carbonyl of the backbone of Val39 (E) of $A\beta_{42}$ protofibril (Fig. 9b). The 2D interaction map display hydrophobic contacts of **6n** with Leu17(D), Phe19(D), Leu17(E), Phe19(E), Gly37(E), Gly38(E), Val39(E), Val40(E), Ile41(E) residues of $A\beta_{42}$ protofibril (Fig. 10b). The molecular docking studies highlighted that **6n** binds preferably to the C-terminus of $A\beta_{42}$, which is known to play a key role in $A\beta_{42}$ aggregation [45], by making hydrogen bonds and hydrophobic contacts with $A\beta_{42}$ residues.

3. Conclusions

By combining the metal chelating triazole moiety and anti-amyloid aggregation pharmacophore, a novel series of compounds **6(a-p)** have been designed, synthesised, and evaluated as multi-target-directed ligands against AD. Among the synthesised library, compound **6n** displayed most potent inhibitory activity against $A\beta_{42}$ aggregation (96.89% inhibition). Compound **6n** inhibited $A\beta_{42}$ aggregation with an IC_{50} value of 8.065 ± 0.129 μM, as compared to the control curcumin (IC_{50} = 6.385 ± 0.009 μM). In addition, **6n** displayed metal-chelating ability and significantly inhibited Cu^{2+}-induced $A\beta_{42}$ aggregation and disassembled preformed Cu^{2+}-induced $A\beta_{42}$ aggregates. Moreover, **6n** successfully controlled the generation of ROS by preventing the copper redox cycle. Compound **6n** is biocompatible as it did not influence the cell viability of the stain (SH-SY5Y cells) significantly even at 50 μM concentration. In addition, **6n** was able to inhibit the toxicity induced by $A\beta_{42}$ aggregates in SH-SY5Y cells. The molecular docking studies highlighted that **6n** bind preferably to the C-terminus region (which is known to play a key role in $A\beta_{42}$ aggregation) of $A\beta_{42}$ by hydrogen bonds and hydrophobic contacts. In summary, a novel triazole-based scaffold has been identified that significantly controls $A\beta_{42}$ aggregation, metal-induced $A\beta_{42}$ aggregation, metal dys-homeostasis, oxidative stress and display neuroprotective action, and might be a promising pharmacotherapeutic lead for further development in AD.

4. Experimental section

4.1. General methods

Human $A\beta_{42}$ was purchased from Anaspec. All the reagents were purchased from Sigma Aldrich and were used without further purification. The progress of the chemical reactions was monitored by thin layer chromatography (TLC) using an appropriate solvent system for development. The reported yields of the synthesised compounds are the isolated yields. In the ^1H NMR the coupling constants (*J*) are given in hertz (Hz) and chemical shifts are stated in parts per million (ppm). The abbreviations s, d, t, m and ABq stand for singlet, doublet, triplet, multiplet and AB quartet, respectively. ^1H NMR (400 MHz or 500 MHz, $CDCl_3$) and ^{13}C NMR (100 MHz or 125 MHz, $CDCl_3$) spectra were recorded on a Bruker NMR spectrometer. HRMS or LRMS data were recorded using Waters Micromass Q-Tof Micro and AB Sciex QTRAP 5500 instrument. Melting points were recorded with a Perfit apparatus. HPLC analysis was recorded on Agilent Technologies 1260 Infinity series system, reverse phase C18 column eluted with 100% acetonitrile at a flow rate 1 mL/min.

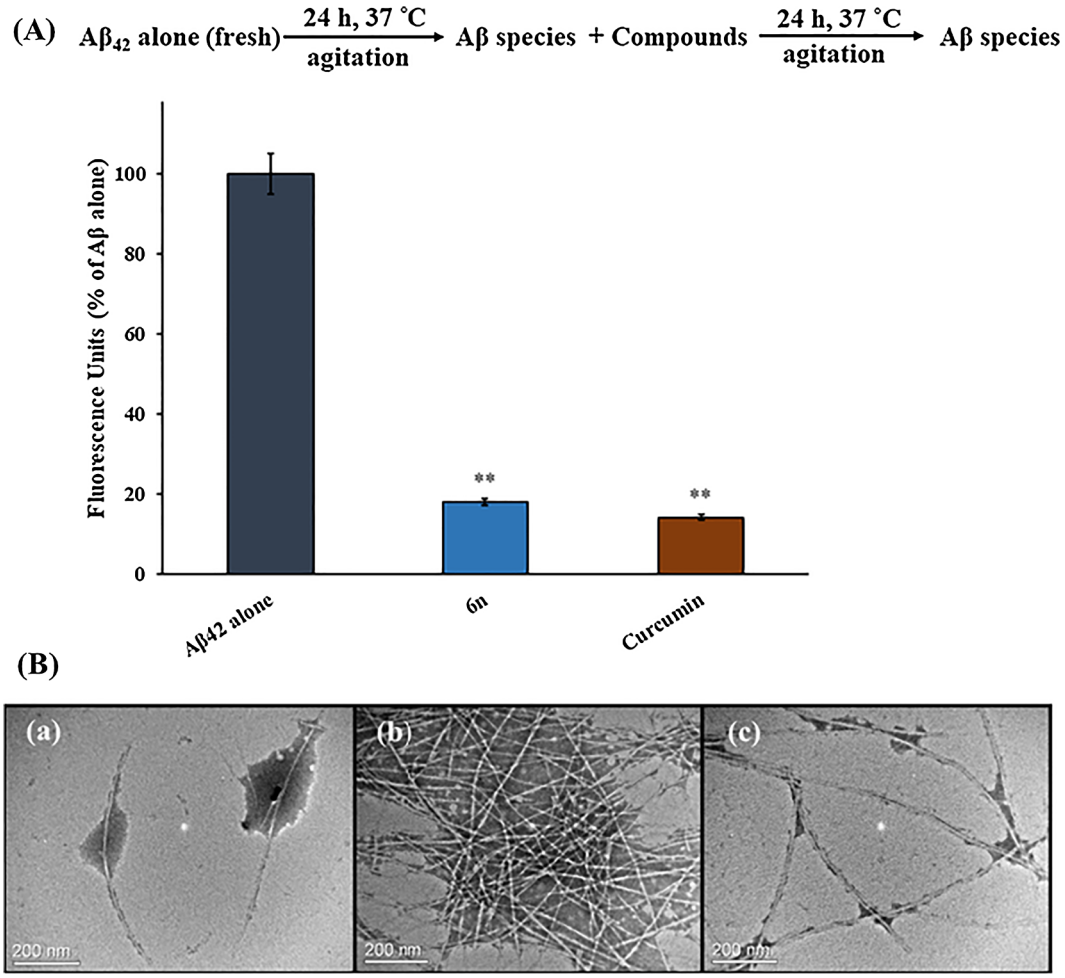

Fig. 3. Disaggregation of self-mediated $A\beta_{42}$ aggregation fibrils by compound **6n**: (A) The results of ThT binding assay. The statistical significance was analysed by one-way analysis of variance (ANOVA) followed by Dunnett's test: (**) $p < 0.01$, versus $A\beta_{42}$ alone. [$A\beta_{42}$] = 20 μM, [**6n**] = [Curcumin] = 40 μM. (B) TEM images of disaggregation of self-mediated $A\beta_{42}$ aggregation fibrils in the presence of compound **6n:** [$A\beta_{42}$] = 20 μM, [**6n**] = 40 μM, 37 °C, 24 h, constant agitation (a) $A\beta_{42}$, 0 h; (b) $A\beta_{42}$, 24 h; (c) $A\beta_{42}$ fibrils + **6n**, 24 h. Scale bar: 200 nm.

*4.2. General procedure for synthesis of di-triazole based amino acids **6(a-p)***

The di-alkyne building block **4** (1 mmol) was dissolved in *t*-BuOH/H_2O (3:3 mL) and the azide **5(a-p)** (2.2 mmol), $Cu(OAc)_2$ (0.2 mmol) and sodium ascorbate (0.4 mmol) were then added. The resulting reaction mixture was stirred at rt till the completion of the reaction (monitored by TLC). The reaction mixture was diluted with ethyl acetate and washed with aq NH_4OH (0.2%) and brine. The aqueous phases were extracted with ethyl acetate (2 × 10 mL). The combined organic extracts were dried over Na_2SO_4 and concentrated *in vacuo*. The

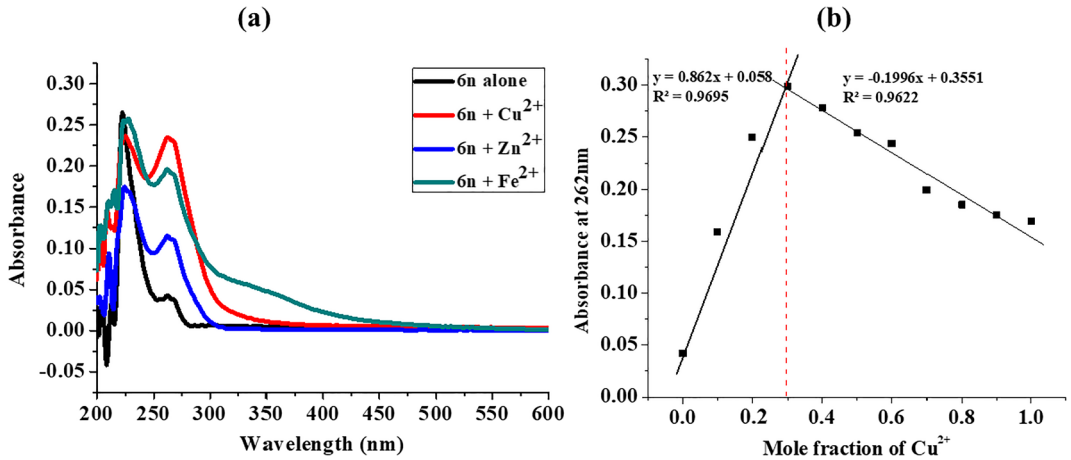

Fig. 4. (a) The UV–Vis spectrum of compound **6n** (20 μM) alone and in the presence of 20 μM $CuSO_4$, $ZnCl_2$ and $FeSO_4$ in buffer (20 mM HEPES, 150 mM NaCl, pH 7.4). (b) Determination of the stoichiometry of **6n**-Cu^{2+} complex by the Job's method.

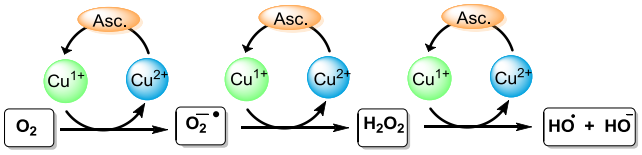

Scheme 2. The schematic representation of formation of hydroxyl radical (OH˙) in the presence of oxygen and ascorbate *via* copper redox cycling.

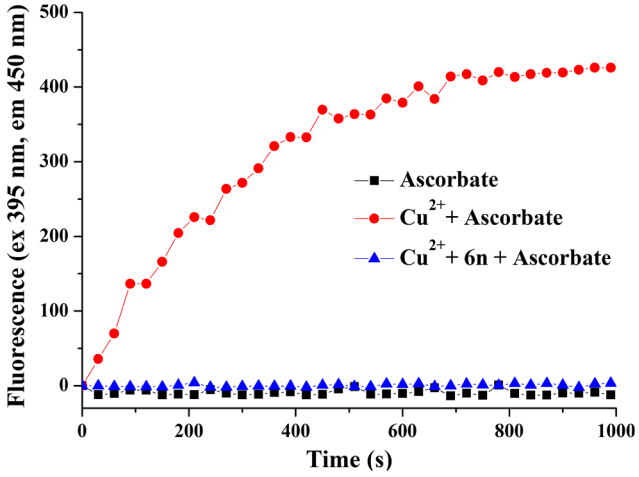

Fig. 5. The fluorescence intensity of 7-hydroxy-CCA in copper-ascorbate and copper ascorbate-**6n** system. CCA = [50 μM] and ascorbate = [150 μM] were incubated in each system. [Cu^{2+}] = [5 μM], [**6n**] = 15 μM, PBS buffer, pH = 7.4, excitation wavelength = 395 nm and emission wavelength = 450 nm.

crude product was purified by flash chromatography on silica gel to afford the pure product.

4.3. Synthesis of compounds 6(a-p)

4.3.1. Compound (6a)

According to the general procedure, di-alkyne **4** (100 mg, 0.45 mmol), phenyl azide **5a** (117.9 mg, 0.99 mmol), $Cu(OAc)_2$ (17.9 mg, 0.09 mmol) and sodium ascorbate (35.7 mg, 0.18 mmol) in *t*-BuOH/H_2O (3:3 mL) was stirred at rt for 24 h. The crude mixture was purified by column chromatography (50% ethyl acetate/petroleum ether) to give compound **6a** (134.4 mg, 65%) as a white solid. R_f: 0.31 (70% ethyl acetate/petroleum ether). Mp: 83–85 °C. ^{1}H NMR (400 MHz, $CDCl_3$): δ = 1.33 (t, J = 7.2 Hz, 3H), 2.01 (s, 3H), 3.49, 3.87 (ABq, J_{AB} = 14.6 Hz, 4H), 4.31 (q, J = 7.2 Hz, 2H), 6.81 (s, 1H), 7.41–7.45 (m, 2H), 7.49–7.54 (m, 4H), 7.69–7.73 (m, 4H), 7.91 (s, 2H) ppm. ^{13}C NMR (100 MHz, $CDCl_3$): δ = 14.13, 14.18, 22.70, 23.98, 29.37, 29.70, 31.08, 31.93, 62.31, 63.16, 120.34, 121.38, 128.69, 129.77, 136.97, 143.32, 170.28, 171.99 ppm. HRMS *m/z*: calcd. for $C_{24}H_{25}N_7O_3Na$ $[M+Na]^+$ 482.1136, found: 482.1917.

4.3.2. Compound (6b)

According to the general procedure, di-alkyne **4** (100 mg, 0.45 mmol), *o*-fluorophenyl azide **5b** (135.6 mg, 0.99 mmol), $Cu(OAc)_2$ (17.9 mg, 0.09 mmol) and sodium ascorbate (35.6 mg, 0.18 mmol) in *t*-BuOH/H_2O (3:3 mL) was stirred at rt for 18 h. The crude mixture was purified by column chromatography (50% ethyl acetate/petroleum ether) to give compound **6b** (182.8 mg, 82%) as a white solid. R_f: 0.30 (70% ethyl acetate/petroleum ether). Mp: 96–98 °C. ^{1}H NMR (400 MHz, $CDCl_3$): δ = 1.36 (t, J = 7.3 Hz, 3H), 1.99 (s, 3H), 3.55, 3.97 (ABq, J_{AB} = 14.5 Hz, 4H), 4.32 (q, J = 7.3 Hz, 2H), 6.62 (s, 1H), 7.27–7.34 (m, 4H), 7.40–7.45 (m, 2H), 7.94–8.01 (m, 4H) ppm. ^{13}C NMR (100 MHz, $CDCl_3$): δ = 14.12, 23.91, 31.14, 62.47, 63.68, 116.91, 117.11, 124.20, 124.29, 124.67, 125.24, 125.28, 130.01, 130.08, 142.97, 151.96, 154.45, 170.25, 171.90. LRMS *m/z*: calcd. for $C_{24}H_{24}F_2N_7O_3$ $[M+H]^+$ 496.5, found: 496.2.

4.3.3. Compound (6c)

According to the general procedure, di-alkyne **4** (100 mg, 0.45 mmol), *m*-fluorophenyl azide **5c** (135.6 mg, 0.99 mmol), $Cu(OAc)_2$ (17.9 mg, 0.09 mmol) and sodium ascorbate (35.6 mg, 0.18 mmol) in *t*-BuOH/H_2O (3:3 mL) was stirred at rt for 12 h. The crude mixture was purified by column chromatography (50% ethyl acetate/petroleum ether) to give compound **6c** (118.2 mg, 53%) as a white solid. R_f: 0.30 (70% ethyl acetate/petroleum ether). Mp: 110–112 °C. ^{1}H NMR (500 MHz, $CDCl_3$): δ = 1.37 (t, J = 7.0 Hz, 3H), 2.03 (s, 3H), 3.49, 3.90 (ABq, J_{AB} = 15.6 Hz, 4H), 4.34 (q, J = 7.0 Hz, 2H), 6.78 (s, 1H), 7.16–7.18 (m, 2H), 7.52–7.55 (m, 6H), 7.93 (s, 2H) ppm. ^{13}C NMR (125 MHz, $CDCl_3$): δ = 14.24, 24.02, 31.14, 62.53, 63.17, 108.16, 115.66, 121.25, 131.29, 143.75, 164.34, 170.31, 172.09 ppm. LRMS *m/z*: calcd. for $C_{24}H_{24}F_2N_7O_3$ $[M+H]^+$ 496.5, found: 496.2.

$$A\beta_{42}\text{ alone (fresh)} + Cu^{2+} \xrightarrow[\text{agitation}]{\text{24 h, 37 °C}} A\beta\text{ species}$$

$$A\beta_{42}\text{ alone (fresh)} + Cu^{2+} \xrightarrow{\text{2 min, rt}} A\beta\text{ species} + \text{compounds} \xrightarrow[\text{agitation}]{\text{24 h, 37 °C}} A\beta\text{ species}$$

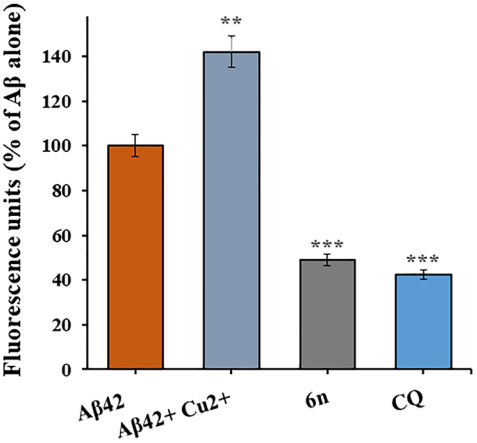

Fig. 6. The inhibition of Cu^{2+}-mediated $A\beta_{42}$ aggregation in the presence of compound **6n**: The results of ThT binding assay. The statistical significance was analysed by one-way analysis of variance (ANOVA) followed by Dunnett's test: (**) $p < 0.01$, (***) $p < 0.001$, versus $A\beta_{42}$ + Cu^{2+} alone. [$A\beta_{42}$] = 20 μM, [Cu^{2+}] = 20 μM, [**6n**] = [CQ] = 40 μM.

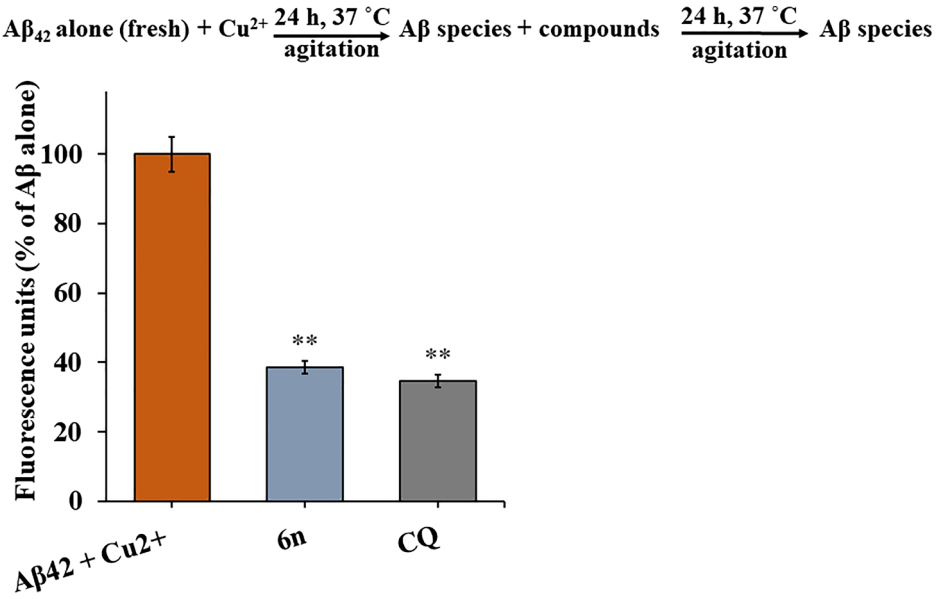

Fig. 7. Disaggregation of Cu^{2+}-mediated $A\beta_{42}$ aggregation in the presence of compound **6n**: The results of ThT binding assay. The statistical significance was analysed by one-way analysis of variance (ANOVA) followed by Dunnett's test: (**) $p < 0.01$, [$A\beta_{42}$] = 20 μM, [Cu^{2+}] = 20 μM, [**6n**] = [CQ] = 40 μM.

4.3.4. Compound (6d)

According to the general procedure, di-alkyne **4** (100 mg, 0.45 mmol), *p*-fluorophenyl azide **5d** (135.6 mg, 0.99 mmol), $Cu(OAc)_2$ (17.9 mg, 0.09 mmol) and sodium ascorbate (35.6 mg, 0.18 mmol) in *t*-BuOH/H_2O (3:3 mL) was stirred at rt for 24 h. The crude mixture was purified by column chromatography (50% ethyl acetate/petroleum ether) to give compound **6d** (196.2 mg, 88%) as a white solid. R_f: 0.33 (70% ethyl acetate/petroleum ether). Mp: 133–135 °C. ^{1}H NMR (500 MHz, $CDCl_3$): δ = 1.36 (t, J = 7.2 Hz, 3H), 2.02 (s, 3H), 3.49, 3.87 (ABq, J_{AB} = 14.5 Hz, 4H), 4.33 (q, J = 7.2 Hz, 2H), 6.82 (s, 1H), 7.18–7.27 (m, 4H), 7.66–7.75 (m, 4H), 7.89 (s, 2H) ppm. ^{13}C NMR (125 MHz, $CDCl_3$): δ = 14.20, 24.00, 31.04, 62.35, 63.06, 116.66, 116.86, 121.58, 122.27, 122.34, 143.47, 170.19, 171.97 ppm. LRMS *m/z*: calcd. for $C_{24}H_{24}F_2N_7O_3$ $[M+H]^+$ 496.5, found: 496.1.

4.3.5. Compound (6e)

According to the general procedure, di-alkyne **4** (100 mg, 0.45 mmol), *o*-chlorophenyl azide **5e** (152.0 mg, 0.99 mmol), $Cu(OAc)_2$ (17.9 mg, 0.09 mmol) and sodium ascorbate (35.6 mg, 0.18 mmol) in *t*-BuOH/H_2O (3:3 mL) was stirred at rt for 12 h. The crude mixture was purified by column chromatography (50% ethyl acetate/petroleum ether) to give compound **6e** (128.3 mg, 54%) as a white solid. R_f: 0.29 (70% ethyl acetate/petroleum ether). Mp: 78–80 °C. ^{1}H NMR (500 MHz, $CDCl_3$): δ = 1.37 (t, J = 7.1 Hz, 3H), 2.02 (s, 3H), 3.58, 3.97 (ABq, J_{AB} = 14.4 Hz, 4H), 4.33 (q, J = 7.1 Hz, 2H), 6.72 (s, 1H), 7.46–7.48 (m, 4H), 7.58–7.61 (m, 2H), 7.64–7.66 (m, 2H), 7.91 (s, 2H) ppm. ^{13}C NMR (125 MHz, $CDCl_3$): δ = 14.20, 24.02, 31.19, 62.44, 63.57, 125.20, 127.20, 127.97, 128.42, 130.68, 130.80, 134.95, 142.40, 170.17, 171.97 ppm. LRMS *m/z*: calcd. for $C_{24}H_{23}Cl_2N_7O_3$ $[M]^+$ 528.4, found: 528.1.

4.3.6. Compound (6f)

According to the general procedure, di-alkyne **4** (100 mg, 0.45 mmol), *m*-chlorophenyl azide **5f** (152.0 mg, 0.99 mmol), $Cu(OAc)_2$ (17.9 mg, 0.09 mmol) and sodium ascorbate (35.6 mg, 0.18 mmol) in *t*-BuOH/H_2O (3:3 mL) was stirred at rt for 24 h. The crude mixture was purified by column chromatography (50% ethyl acetate/petroleum ether) to give compound **6f** (168.8 mg, 71%) as a white solid. R_f: 0.23 (70% ethyl acetate/petroleum ether). Mp: 97–99 °C. ^{1}H NMR (500 MHz, $CDCl_3$): δ = 1.37 (t, J = 7.3 Hz, 3H), 2.03 (s, 3H), 3.49, 3.89 (ABq, J_{AB} = 14.2 Hz, 4H), 4.34 (q, J = 7.3 Hz, 2H), 6.79 (s, 1H), 7.42–7.44 (m, 2H), 7.46–7.50 (m, 2H), 7.62–7.64 (m, 2H), 7.79 (s, 2H), 7.92 (s, 2H) ppm. ^{13}C NMR (125 MHz, $CDCl_3$): δ = 14.26, 24.06, 31.07, 62.44, 63.10, 118.26, 120.63, 121.31, 128.78, 130.85, 135.66, 137.77, 143.61, 170.21, 171.93 ppm. LRMS *m/z*: calcd. for $C_{24}H_{23}Cl_2N_7O_3$ $[M]^+$ 528.4, found: 528.1.

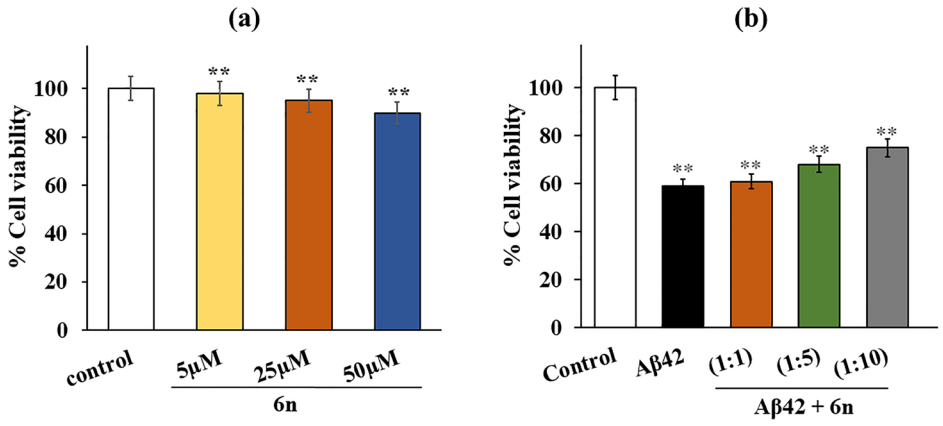

Fig. 8. MTT cell viability assay: (a) Cell viability in the presence of **6n** alone at variable concentrations (5 μM, 25 μM and 50 μM) after 48 h of incubation. (b) Cell viability in the presence of $A\beta_{42}$ alone at a concentration of 5 μM and mixture of $A\beta_{42}$-**6n** at molar ratios of 1:1, 1:5, 1:10. The data is expressed as mean values ± SEM from three independent experiments. The statistical significance was analysed by one-way analysis of variance (ANOVA) followed by Dunnett's test: (**) $p < 0.01$, In both panel (a) and (b) error bars represent the average of three replicate experiments.

Table 2
Molecular docking analysis of compound **6n** with $A\beta_{42}$ monomer and protofibril structure.

Compound	Protein structure[a]	AutoDock binding energy (kcal/mol)	$A\beta_{42}$ residues involved in intermolecular hydrogen bonding			$A\beta_{42}$ residues involved in intermolecular hydrophobic contacts
			Residue	Atom[b]	Distance (nm)	
6n	$A\beta_{42}$ monomer	−5.52	Ala42	N: HN	0.19	Ala30, Ile31, Leu34, Met35, Gly38, Val39, Val40, Ile41, Ala42
6n	$A\beta_{42}$ protofibril	−6.75	Ile41(E)	N: HN	0.19	Leu17(D), Phe19(D), Leu17(E), Phe19(E), Gly37(E), Gly38(E), Val39(E), Val40(E), Ile41(E)
			Val39(E)	NH: O	0.20	

[a] The PDB ID for $A\beta_{42}$ monomer and $A\beta_{42}$ protofibril used in the present study are 1ZOQ, and 2BEG, respectively.
[b] The atoms on left represent ligand atoms, and on the right represent $A\beta_{42}$ residue atoms.

4.3.7. Compound (6g)

According to the general procedure, di-alkyne **4** (100 mg, 0.45 mmol), *p*-chlorophenyl azide **5 g** (152.0 mg, 0.99 mmol), $Cu(OAc)_2$ (17.9 mg, 0.09 mmol) and sodium ascorbate (35.6 mg, 0.18 mmol) in *t*-BuOH/H_2O (3:3 mL) was stirred at rt for 12 h. The crude mixture was purified by column chromatography (50% ethyl acetate/petroleum ether) to give compound **6 g** (128.4 mg, 54%) as a white solid. R_f: 0.30 (70% ethyl acetate/petroleum ether). Mp: 98–100 °C. ^{1}H NMR (500 MHz, $CDCl_3$): δ = 1.36 (t, J = 7.2 Hz, 3H), 2.02 (s, 3H), 3.49, 3.89 (ABq, J_{AB} = 14.8 Hz, 4H), 4.34 (q, J = 7.2 Hz, 2H), 6.79 (s, 1H), 7.51–7.55 (m, 4H), 7.68–7.70 (m, 4H), 7.91 (s, 2H) ppm. ^{13}C NMR (125 MHz, $CDCl_3$): δ = 14.11, 24.15, 32.66, 61.26, 62.15, 121.32, 121.50, 123.41, 129.98, 130.79, 132.82, 140.83, 170.44, 171.20 ppm. LRMS *m/z*: calcd. for $C_{24}H_{23}Cl_2N_7O_3$ $[M]^+$ 528.4, found: 528.1.

4.3.8. Compound (6h)

According to the general procedure, di-alkyne **4** (100 mg, 0.45 mmol), *o*-bromophenyl azide **5 h** (196.0 mg, 0.99 mmol), $Cu(OAc)_2$ (17.9 mg, 0.09 mmol) and sodium ascorbate (35.6 mg, 0.18 mmol) in *t*-BuOH/H_2O (3:3 mL) was stirred at rt for 8 h. The crude mixture was purified by column chromatography (50% ethyl acetate/petroleum ether) to give compound **6 h** (144.5 mg, 52%) as a white solid. R_f: 0.33 (70% ethyl acetate/petroleum ether). Mp: 73–75 °C. ^{1}H NMR (500 MHz, $CDCl_3$): δ = 1.37 (t, J = 7.1 Hz, 3H), 2.03 (s, 3H), 3.58, 3.97 (ABq, J_{AB} = 14.2 Hz, 4H), 4.32 (q, J = 7.1 Hz, 2H), 6.75 (s, 1H), 7.40–7.43 (m, 2H), 7.49–7.52 (m, 2H), 7.56–7.58 (m, 2H), 7.76–7.78 (m, 2H), 7.86 (s, 2H) ppm. ^{13}C NMR (125 MHz, $CDCl_3$): δ = 14.22, 24.14, 31.15, 62.44, 63.55, 118.56, 125.31, 128.20, 128.55, 131.13, 133.92, 136.58, 142.30, 170.09, 171.89 ppm. LRMS *m/z*: calcd. for $C_{24}H_{24}Br_2N_7O_3$ $[M+H]^+$ 618.3, found: 618.0.

4.3.9. Compound (6i)

According to the general procedure, di-alkyne **4** (100 mg, 0.45 mmol), *m*-bromophenyl azide **5i** (196.0 mg, 0.99 mmol), $Cu(OAc)_2$ (17.9 mg, 0.09 mmol) and sodium ascorbate (35.6 mg, 0.18 mmol) in *t*-BuOH/H_2O (3:3 mL) was stirred at rt for 20 h. The crude mixture was purified by column chromatography (50% ethyl acetate/petroleum ether) to give compound **6i** (161.1 mg, 58%) as a white solid. R_f: 0.31 (70% ethyl acetate/petroleum ether). Mp: 96–98 °C. ^{1}H NMR (500 MHz, $CDCl_3$): δ = 1.37 (t, J = 7.2 Hz, 3H), 2.03 (s, 3H), 3.49, 3.89 (ABq, J_{AB} = 14.6 Hz, 4H), 4.34 (q, J = 7.2 Hz, 2H), 6.79 (s, 1H), 7.40–7.43 (m, 2H), 7.58–7.59 (m, 2H), 7.67–7.68 (m, 2H), 7.91 (s, 2H), 7.95 (s, 2H) ppm. ^{13}C NMR (125 MHz, $CDCl_3$): δ = 14.24, 24.15, 31.14, 62.53, 63.17, 118.84, 121.38, 123.54, 131.17, 131.80, 137.90, 143.75, 172.90 ppm. LRMS *m/z*: calcd. for $C_{24}H_{24}Br_2N_7O_3$ $[M+H]^+$ 618.3, found: 618.0.

4.3.10. Compound (6j)

According to the general procedure, di-alkyne **4** (100 mg, 0.45 mmol), *p*-bromophenyl azide **5j** (196.0 mg, 0.99 mmol), $Cu(OAc)_2$ (17.9 mg, 0.09 mmol) and sodium ascorbate (35.6 mg, 0.18 mmol) in *t*-BuOH/H_2O (3:3 mL) was stirred at rt for 6 h. The crude mixture was purified by column chromatography (50% ethyl acetate/petroleum ether) to give compound **6j** (147.2 mg, 53%) as a white solid. R_f: 0.30 (70% ethyl acetate/petroleum ether). Mp: 108–110 °C. ^{1}H NMR (400 MHz, $CDCl_3$): δ = 1.30 (t, J = 7.1 Hz, 3H), 2.06 (s, 3H), 3.58, 3.81 (ABq, J_{AB} = 14.8 Hz, 4H), 4.28 (q, J = 7.1 Hz, 2H), 7.48 (s, 1H), 7.57–7.75 (m, 8H), 8.19 (s, 2H) ppm. ^{13}C NMR (100 MHz, $CDCl_3$): δ = 14.13, 23.63, 30.84, 62.39, 121.80, 122.05, 122.58, 123.20, 133.09, 135.45, 142.59, 170.76, 171.37 ppm. HRMS *m/z*: *m/z*: calcd. for $C_{24}H_{23}Br_2N_7O_3Na$ $[M+Na]^+$ 640.2823, found: 639.9523.

4.3.11. Compound (6k)

According to the general procedure, di-alkyne **4** (100 mg, 0.45 mmol), *o*-iodophenyl azide **5 k** (242.6 mg, 0.99 mmol), $Cu(OAc)_2$ (17.9 mg, 0.09 mmol) and sodium ascorbate (35.6 mg, 0.18 mmol) in *t*-BuOH/H_2O (3:3 mL) was stirred at rt for 30 h. The crude mixture was

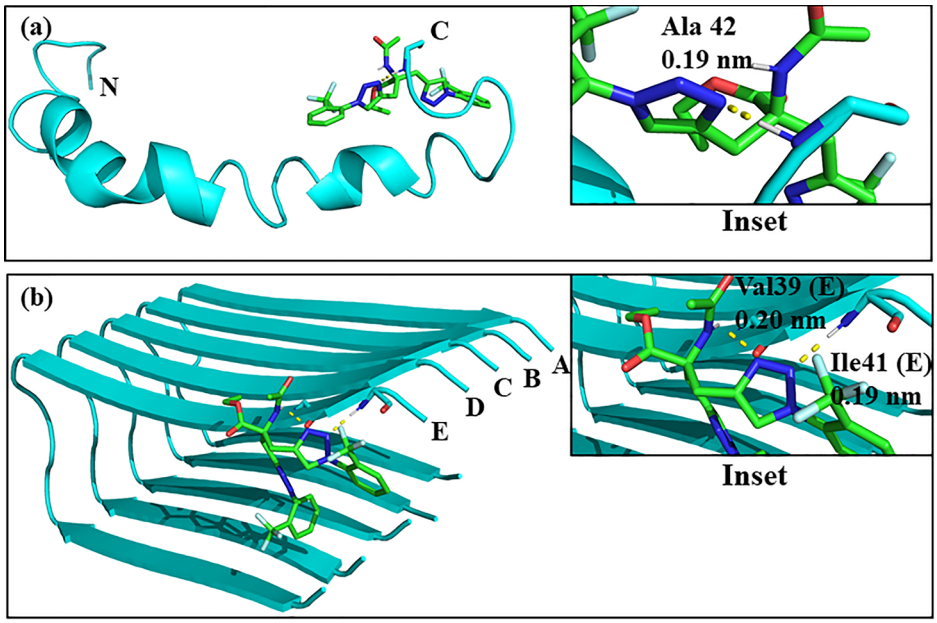

Fig. 9. The docked complex of **6n** with $A\beta_{42}$ monomer (PDB ID: 1Z0Q) and $A\beta_{42}$ protofibril (PDB ID: 2BEG) are shown in panel (a), and (b), respectively. The N- and C-terminal is labelled in $A\beta_{42}$ monomer structure shown in panel (a). The $A\beta_{42}$ protofibril structure with five peptide chains, A–E, is shown in the cartoon representation in cyan and **6n** is shown in the stick representation. The hydrogen bonds between $A\beta_{42}$ monomer-**6n**, and $A\beta_{42}$ protofibril-**6n** are shown as yellow dashed lines with distance in nm in panel (a), and (b), respectively.

purified by column chromatography (50% ethyl acetate/petroleum ether) to give compound **6 k** (188.8 mg, 59%) as a white solid. R_f: 0.31 (70% ethyl acetate/petroleum ether). Mp: 77–79 °C. ^{1}H NMR (500 MHz, $CDCl_3$): δ = 1.37 (t, J = 7.1 Hz, 3H), 2.05 (s, 3H), 3.58, 3.96 (ABq, J_{AB} = 14.4 Hz, 4H), 4.33 (q, J = 7.1 Hz, 2H), 6.79 (s, 1H), 7.24–7.27 (m, 2H), 7.45–7.46 (m, 2H), 7.51–7.54 (m, 2H), 7.78 (s, 2H), 8.05–8.02 (m, 2H) ppm. ^{13}C NMR (125 MHz, $CDCl_3$): δ = 14.36, 24.40, 31.27, 62.53, 63.55, 94.05, 125.32, 127.99, 129.39, 131.55, 140.32, 142.48, 170.19, 171.97 ppm. LRMS *m/z*: calcd. for $C_{24}H_{24}I_2N_7O_3$ $[M+H]^+$ 712.3, found 712.0.

4.3.12. Compound (6l)

According to the general procedure, di-alkyne **4** (100 mg, 0.45 mmol), *m*-iodophenyl azide **5 l** (242.6 mg, 0.99 mmol), $Cu(OAc)_2$ (17.9 mg, 0.09 mmol) and sodium ascorbate (35.6 mg, 0.18 mmol) in *t*-BuOH/H_2O (3:3 mL) was stirred at rt for 20 h. The crude mixture was purified by column chromatography (50% ethyl acetate/petroleum ether) to give compound **6 l** (188.8 mg, 59%) as a pale yellow solid. R_f: 0.31 (70% ethyl acetate/petroleum ether). Mp: 94–96 °C. ^{1}H NMR (400 MHz, $CDCl_3$): δ = 1.34 (t, J = 7.2 Hz, 3H), 2.01 (s, 3H), 3.48, 3.86 (ABq, J_{AB} = 14.5 Hz, 4H), 4.31 (q, J = 7.2 Hz, 2H), 6.79 (s, 1H),

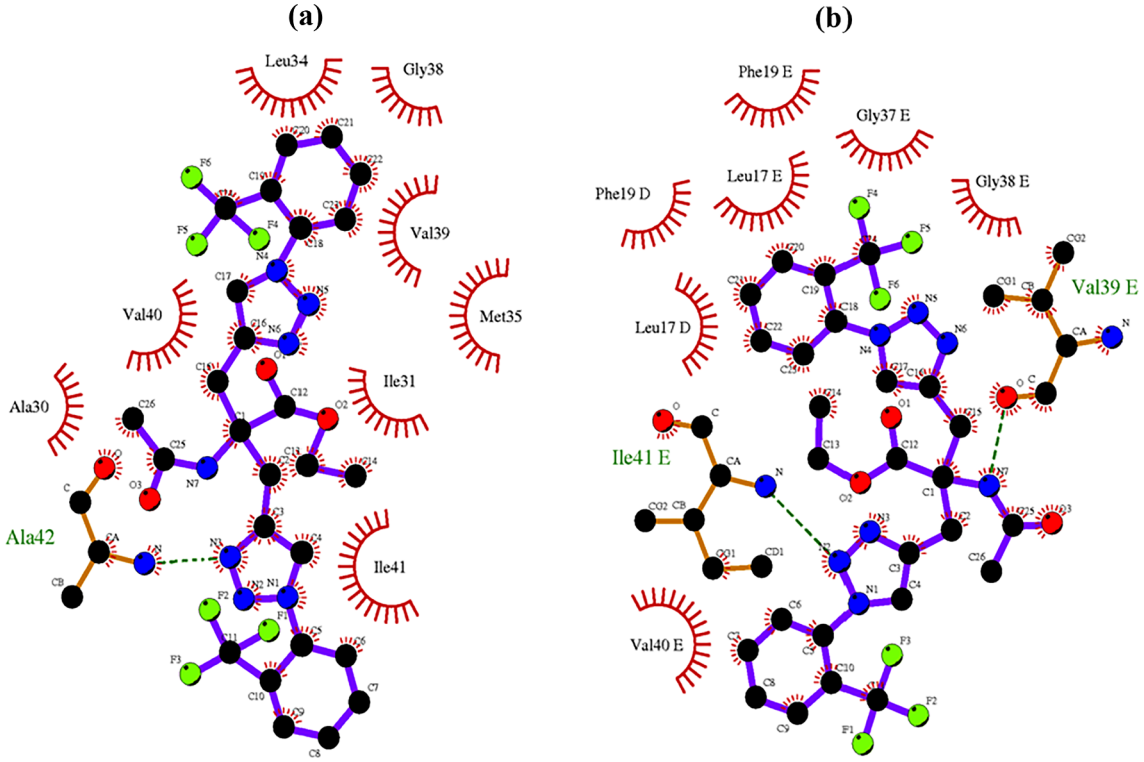

Fig. 10. The 2D interaction maps displaying the hydrophobic contacts of **6n** with $A\beta_{42}$ monomer (PDB ID: 1Z0Q) and $A\beta_{42}$ protofibril (PDB ID: 2BEG) are shown in panel (a), and (b), respectively. The maps are generated using LigPlot + software. The hydrogen bonds between $A\beta_{42}$ monomer-**6n** and $A\beta_{42}$ protofibril-**6n** are shown as green lines.

7.22–7.24 (m, 2H), 7.67–7.70 (m, 2H), 7.75–7.77 (m, 2H), 7.88 (s, 2H), 8.08–8.10 (m, 2H) ppm. ^{13}C NMR (100 MHz, $CDCl_3$): δ = 14.12, 23.92, 31.14, 62.47, 63.68, 124.20, 124.29, 124.67, 125.24, 125.27, 130.01, 142.97, 151.96, 170.25, 171.90 ppm. LRMS *m/z*: calcd. for $C_{24}H_{24}I_2N_7O_3$ $[M+H]^+$ 712.3, found 712.1.

4.3.13. Compound (6m)

According to the general procedure, di-alkyne **4** (100 mg, 0.45 mmol), *p*-iodophenyl azide **5 m** (242.6 mg, 0.99 mmol), $Cu(OAc)_2$ (17.9 mg, 0.09 mmol) and sodium ascorbate (35.6 mg, 0.18 mmol) in *t*-BuOH/H_2O (3:3 mL) was stirred at rt for 24 h. The crude mixture was purified by column chromatography (50% ethyl acetate/petroleum ether) to give compound **6 m** (208.1 mg, 65%) as a white solid. R_f: 0.31 (70% ethyl acetate/petroleum ether). Mp: 113–115 °C. ^{1}H NMR (400 MHz, $CDCl_3$): δ = 1.33 (t, J = 7.0 Hz, 3H), 1.98 (s, 3H), 3.46, 3.85 (ABq, J_{AB} = 14.6 Hz, 4H), 4.30 (q, J = 7.0 Hz, 2H), 6.77 (s, 1H), 7.46–7.49 (m, 4H), 7.83–7.85 (m, 4H), 7.88 (s, 2H) ppm. ^{13}C NMR (100 MHz, $CDCl_3$): δ = 14.17, 23.95, 29.70, 31.04, 62.38, 63.10, 93.51, 121.12, 121.82, 136.51, 138.82, 143.59, 170.30 ppm. LRMS *m/z*: calcd. for $C_{24}H_{24}I_2N_7O_3$ $[M+H]^+$ 712.3, found 712.1.

4.3.14. Compound (6n)

According to the general procedure, di-alkyne **4** (100 mg, 0.45 mmol), *o*-trifluoromethylphenyl azide **5n** (185.3 mg, 0.99 mmol), $Cu(OAc)_2$ (17.9 mg, 0.09 mmol) and sodium ascorbate (35.6 mg, 0.18 mmol) in *t*-BuOH/H_2O (3:3 mL) was stirred at rt for 24 h. The crude mixture was purified by column chromatography (50% ethyl acetate/petroleum ether) to give compound **6n** (176.9 mg, 66%) as a white solid. R_f: 0.29 (70% ethyl acetate/petroleum ether). Mp: 78–80 °C. ^{1}H NMR (400 MHz, $CDCl_3$): δ = 1.34 (t, J = 7.1 Hz, 3H), 1.98 (s, 3H), 3.54, 3.96 (ABq, J_{AB} = 14.5 Hz, 4H), 4.30 (q, J = 7.1 Hz, 2H), 6.65 (s, 1H), 7.55–7.57 (m, 2H), 7.65–7.76 (m, 6H), 7.84–7.86 (m, 2H) ppm. ^{13}C NMR (100 MHz, $CDCl_3$): δ = 14.24, 23.77, 31.27, 62.66, 63.80, 126.08, 127.61, 129.01, 130.66, 133.46, 135.23, 142.61, 170.44, 171.84 ppm. HRMS *m/z*: calcd. for $C_{26}H_{24}F_6N_7O_3$ $[M+H]^+$ 596.5042, found: 596.5984. HPLC purity: 99.98%.

4.3.15. Compound (6o)

According to the general procedure, di-alkyne **4** (100 mg, 0.45 mmol), *m*-trifluoromethylphenyl azide **5o** (185.3 mg, 0.99 mmol), $Cu(OAc)_2$ (17.9 mg, 0.09 mmol) and sodium ascorbate (35.6 mg, 0.18 mmol) in *t*-BuOH/H_2O (3:3 mL) was stirred at rt for 10 h. The crude mixture was purified by column chromatography (50% ethyl acetate/petroleum ether) to give compound **6o** (150.1 mg, 56%) as a white solid. R_f: 0.30 (70% ethyl acetate/petroleum ether). Mp: 96–98 °C. ^{1}H NMR (400 MHz, $CDCl_3$): δ = 1.35 (t, J = 7.2 Hz, 3H), 1.99 (s, 3H), 3.49, 3.89 (ABq, J_{AB} = 14.5 Hz, 4H), 4.32 (q, J = 7.2 Hz, 2H), 6.78 (s, 1H), 7.64–7.71 (m, 4H), 7.93–7.90 (m, 2H), 7.97 (s, 2H), 8.02 (s, 2H) ppm. ^{13}C NMR (100 MHz, $CDCl_3$): δ = 14.18, 24.19, 31.00, 62.55, 63.11, 117.46, 121.35, 123.44, 125.38, 130.67, 137.20, 143.87, 170.28, 171.95 ppm. HRMS *m/z*: calcd. for $C_{26}H_{24}F_6N_7O_3$ $[M+H]^+$ 596.5042, found: 596.1830.

4.3.16. Compound (6p)

According to the general procedure, di-alkyne **4** (100 mg, 0.45 mmol), *p*-trifluoromethylphenyl azide **5p** (185.3 mg, 0.99 mmol), $Cu(OAc)_2$ (17.9 mg, 0.09 mmol) and sodium ascorbate (35.6 mg, 0.18 mmol) in *t*-BuOH/H_2O (3:3 mL) was stirred at rt for 12 h. The crude mixture was purified by column chromatography (50% ethyl acetate/petroleum ether) to give compound **6p** (142.0 mg, 53%) as a white solid. R_f: 0.30 (70% ethyl acetate/petroleum ether). Mp: 116–118 °C. ^{1}H NMR (500 MHz, $CDCl_3$): δ = 1.36 (t, J = 7.1 Hz, 3H), 2.02 (s, 3H), 3.48, 3.87 (ABq, J_{AB} = 14.8 Hz, 4H), 4.33 (q, J = 7.1 Hz, 2H), 6.81 (s, 1H), 7.22–7.23 (m, 4H), 7.70–7.72 (m, 4H), 7.89 (s, 2H) ppm. ^{13}C NMR (100 MHz, $CDCl_3$): δ = 14.18, 24.47, 31.28, 61.30, 63.25, 116.90, 120.19, 121.63, 123.02, 125.99, 143.73, 170.56, 171.12 ppm. LRMS *m/z*: calcd. for $C_{26}H_{24}F_6N_7O_3$ $[M+H]^+$ 596.5, found: 596.1.

4.4. Thioflavin T (ThT) fluorescence assay

$A\beta_{42}$ peptide was purchased from Anaspec and dissolved in 1,1,1,3,3,3-hexafluoro-2-propanol (HFIP). HFIP treated $A\beta_{42}$ peptide was further evaporated and stored at −20 °C. The stock solution of $A\beta_{42}$ (221.5 μM) was prepared by dissolving 0.1 mg $A\beta_{42}$ in 100 μL NaOH (10 mM) and stored at −80 °C for further use. Then 2 mM stock solutions of all the test compounds and controls were prepared in DMSO. 1 mM stock solution of ThT was prepared in 50 mM PBS buffer (pH 7.4) then diluted to 200 μM stock. For self-induced aggregation assay, mixture of $A\beta_{42}$ (18 μL, 20 μM) and ThT (20 μL, 20 μM) with or without the presence of test compounds (5 μL, 100 μM) were diluted to final volume of 200 μL with 50 mM PBS buffer (pH 7.4) in black 96-well plate and incubated for 24 h at 37 °C with constant agitation (180 rpm). The final concentration of DMSO was kept constant at 2.5% (v/v). For disaggregation assay, the monomer $A\beta_{42}$ was incubated for 24 h at 37 °C to form fibrils. Then, the test compounds were added to the aliquots of $A\beta_{42}$ fibrils. The aliquot of $A\beta_{42}$ fibrils alone or with test compound were incubated for another 24 h under same conditions. The fluorescence intensities were recorded using a SpectraMax M5^e spectrophotometer with excitation and emission wavelengths at 450 nm and 485 nm respectively. Percentage inhibition was calculated by using the formula $(1–F_{sample}/F_{control}) * 100$.

For the inhibition of Cu^{2+}-mediated $A\beta_{42}$ aggregation, the $A\beta_{42}$ stock solution was diluted in 20 μM HEPES (pH 6.6) with 150 μM NaCl. The mixture of the $A\beta_{42}$ (18 μL, 20 μM) with copper (2.5 μL, 25 μM) and with or without the presence of the test compounds (5 μL, 40 μM) were incubated at 37 °C for 24 h. Then 25.5 μL of the sample was diluted to a final volume of 200 μL with 50 mM glycine − NaOH buffer (pH 8.0) containing thioflavin T (20 μM). For disaggregation assay, the monomer $A\beta_{42}$ was incubated with copper for 24 h at 37 °C to form fibrils. Then, the test compounds were added to the aliquots of $A\beta_{42}$ fibrils. The aliquot of $A\beta_{42}$ fibrils in the absence or presence of test compound were incubated for another 24 h under same conditions.

4.5. Statistical analysis

Statistical analysis was performed with one-way analysis of variance (ANOVA) followed by Dunnett's test on at least three different measurements ($^{**}p < 0.01$, $^{***}p < 0.001$; Mean ± SD for n = 3 experiments). ThT Data analysis and graph production was done by using IBM SPSS Statistics (version 21) for Windows.

4.6. Transmission electron microscopy assay

Transmission electron microscopy was performed to visualize $A\beta_{42}$ fibrils in the presence of compound **6n**. For self-induced $A\beta_{42}$ aggregation assay, $A\beta_{42}$ monomer (20 μM) was incubated alone or in the presence of **6n** (40 μM) in 50 mM PBS buffer (pH 7.4) at 37 °C for 24 h. For $A\beta_{42}$ disaggregation assay, $A\beta_{42}$ fibrils (20 μM) was incubated in the presence of **6n** (40 μM) in 50 mM PBS buffer (pH 7.4) at 37 °C for 24 h. 5 μL of the samples were placed on a carbon-coated 200 mesh (agar scientific) copper grid for 2 min and allowed to dry for 30 mins. Each grid was stained with 2% phosphotungstic acid for 45 s. After draining off the excess staining solution, the specimen was loaded to grid holder and transferred for imaging by transmission electron microscopy (JEOL JEM-2100) operating at 200 kV.

4.7. Metal chelating studies

The chelating ability of compound **6n** towards biometals such as Cu^{2+}, Zn^{2+} and Fe^{2+} was examined by UV–Vis spectroscopy (Ultrospec 3000). The stock solution of compound **6n** (4 mM), metal ions (8 mM)

were prepared in methanol. The solution of **6n** (20 μM, final concentration) alone or in the presence of $CuSO_4$, $ZnCl_2$ or $FeSO_4$ (20 μM, final concentration) in (20 mM HEPES, 150 mM NaCl, pH 7.4) were incubated for 30 min at 25 °C. The spectra of each sample were recorded with wavelength ranging from 200 nm to 600 nm using blank containing 20 mM HEPES, 150 mM NaCl, pH 7.4.

The stoichiometry of the **6n**-Cu^{2+} complex was determined by Job's method, by preparing the separate solutions of **6n** and $CuSO_4$ in which the total concentration remain constant (40 μM) but the proportion of each component was varied from 0% to 100%. The absorbance at 262 nm was plotted against mole fraction of Cu^{2+}. The breakpoint displays the stoichiometry of the complex.

4.8. Ascorbate assay

The ascorbate study was performed by using SpectraMax M5^e spectrophotometer. The fluorescence intensities were recorded with excitation and emission wavelengths at 395 nm and 450 nm for the period of 16 min. The stock solution of **6n** (in methanol), $CuSO_4$ (in Milli-Q water), CCA and ascorbate were dissolved and diluted in 50 mM PBS buffer (pH 7.4). The final volume of the sample is 200 μL. The production of hydroxyl radical was measured as the change of CCA into 7-hydroxy-CCA. The order of addition follows: CCA (50 μM), ligand (15 μM), or copper (5 μM) and ascorbate (150 μM). All test solutions contained 1 μM desferryl.

4.9. MTT cell viability assay

The potential role of **6n** in the $A\beta_{42}$-induced cell toxicity was studied using the MTT assay with SH-SY5Y cell line according to the literature procedure [44]. In high glucose Dulbecco's modified eagle's medium (DMEM) supplemented with 10% FBS, 100 U/mL penicillin and 100 U/mL streptomycin, the SH-SY5Y cells were maintained at 37 °C under 5% CO_2 in a CO_2 cell culture box. In a polystyrene 96-well plate, a total of 5×10^3 cells (90 μL) were seeded for 24 h and then, the cells were treated with $A\beta_{42}$ and **6n** + $A\beta_{42}$ [2.5 μL, **6n** of different concentration was co-incubated with $A\beta_{42}$ (2.25 μL) monomers at 37 °C for 24 h]. The final concentration of DMSO was kept constant at 2.5% (v/v). For The incubation of cells was continued for an additional 24 h, and then 10 μL of MTT solution at the concentration of 5.5 mg/mL in PBS was added into each well and followed by another 4 h of incubation. Then the medium was discarded, and 100 μL of DMSO was used to dissolve the cells till the complete dissolution of purple crystals. By plate reader, the absorbance at 570 nm was measured. From each reading, the background was subtracted *i.e.* the wells containing only medium. The data obtained was normalized as a percentage of the control group without $A\beta_{42}$ and inhibitor.

4.10. Molecular docking studies

The molecular docking was performed using AutoDock 4.2 [46]. To identify the binding region and key interactions of **6n** with $A\beta_{42}$ using molecular docking, the NMR structure of $A\beta_{42}$ monomer (PDB ID: 1Z0Q) and $A\beta_{42}$ protofibril (PDB ID: 2BEG) were employed. The 3D structure of **6n** was optimized by Gaussian using Hatree–Fock (HF) theory with basis set 6-31G(d). The grid spacing was kept default (0.375 Å) and dimension of the box for 1Z0Q was set to 127 Å × 73 Å × 69 Å with grid center defined at x = −1.733, y = 1.693, and z = −6.759. For 2BEG, the dimension of the box was set to 126 Å × 72 Å × 86 Å with grid center defined at x = −0.200, y = 0.250, and z = −8.949. The population of 150 individuals was employed to generate 100 conformations for 27,000 generations with 2,500,000 energy evaluations. The mutation rate of 0.02, a crossover rate of 0.80, and reference root-mean-square deviation (RMSD) were kept as default. The Lamarckian Genetic Algorithm that utilizes global search (Genetic Algorithm) and local search (Solis and Wets algorithm) was chosen for the present study [47]. The docked poses of **6n** were clustered using a tolerance of 0.2 nm for RMSD and ranked on the basis of binding energy.

Acknowledgments

DG is thankful to Science and Engineering Research Board (SERB), Department of Science & Technology (DST), Government of India for the award of SERB Young Scientists Research Grant (File No. YSS/2015/000320). AK gratefully acknowledges SERB-DST, India for the award of research fellowship. The authors acknowledge Department of Chemistry and Department of Biotechnology, Sri Guru Granth Sahib World University, Fatehgarh Sahib, Punjab, India and School of Chemistry and Biochemistry, Thapar Institute of Engineering & Technology, Patiala, Punjab, India for providing the research facilities. The authors express sincere gratitude toward National Agri-Food Biotechnology Institute, S.A.S. Nagar, Punjab, India for permitting us to use the instrumental facilities.

Appendix A. Supplementary material

Supplementary data to this article can be found online at https://doi.org/10.1016/j.bioorg.2019.03.058.

References

[1] A. Alzheimer, ÜberEineEigenartigeErkrankung Der Hirnrinde, Allg. Zschr. Psychiat. Psych. gerichtl. Med. 64 (1907) 146–148.
[2] (a) WHO, Dementia, 2018. http://www.who.int/news-room/fact-sheets/detail/dementia; (b) https://www.alz.co.uk/research/WorldAlzheimerReport2016.pdf.
[3] A. Rauk, The chemistry of Alzheimer's disease, Chem. Soc. Rev. 38 (2009) 2698–2715.
[4] http://www.alzforum.org/therapeutics/rivastigmine.
[5] (a) http://www.alzforum.org/therapeutics/donepezil. (b) J. Meunier, J. Ieni, T. Maurice, The anti–amnesic and neuroprotective effects of donepezil against amyloid β25–35 peptide–induced toxicity in mice involve an interaction with the σ1 receptor, Br. J. Pharmacol. 149 (2006) 998–1012
[6] http://www.alzforum.org/therapeutics/galantamine.
[7] http://www.alzforum.org/therapeutics/memantine.
[8] R.A. Hansen, G. Gartlehner, A.P. Webb, L.C. Morgan, C.G. Moore, D.E. Jonas, Efficacy and safety of donepezil, galantamine, and rivastigmine for the treatment of Alzheimer's disease: a systematic review and meta–analysis, Clin. Interv. Aging 3 (2008) 211–225.
[9] http://www.pharmacodia.com/web/drug/1_3088.html#clinical_trial.
[10] http://www.alzforum.org/news/research–news/tau–targeting––drug–davunetide–washes–out–phase–3–trials.
[11] R.C. Green, L.S. Schneider, D.A. Amato, A.P. Beelen, G. Wilcock, E.A. Swabb, K.H. Zavitz, Effect of tarenflurbil on cognitive decline and activities of daily living in patients with mild Alzheimer disease: a randomized controlled trial, JAMA 302 (2009) 2557–2564.
[12] R.S. Doody, R. Raman, M. Farlow, T. Iwatsubo, B. Vellas, S. Joffe, K. Kieburtz, F. He, X. Sun, R.G. Thomas, P.S. Aisen, A phase 3 trial of semagacestat for treatment of Alzheimer's disease, N. Engl. J. Med. 369 (2013) 341–350.
[13] V. Coric, S. Salloway, C. van Dyck, W. Kerselaers, S. Kaplita, C. Curtis, J. Ross, R.W. Richter, N. Andreasen, M. Brody, S.K. Sharma, J.M. Cedarbaum, R.M. Berman, Phase II study of the gamma–secretase inhibitor avagacestat (BMS–708163) in predementia Alzheimer's disease, Alzheimers Dement. 9 (2013) 283.
[14] http://www.alzforum.org/new/detail.asp?id535222013.
[15] E. Liu, M.E. Schmidt, R. Margolin, R. Sperling, R. Koeppe, N.S. Mason, W.E. Klunk, C.A. Mathis, S. Salloway, N.C. Fox, D.L. Hill, A.S. Les, P. Collins, K.M. Gregg, J. Di, Y. Lu, I.C. Tudor, B.T. Wyman, K. Booth, S. Broome, E. Yuen, M. Grundman, H.R. Brashear, Bapineuzumab 301 and 302 Clinical Trial Investigators, Amyloid–β 11C–PiB–PET imaging results from 2 randomized bapineuzumab phase 3 AD trials, Neurology 85 (2015) 692–700.
[16] R.S. Doody, R.G. Thomas, M. Farlow, T. Iwatsubo, B. Vellas, S. Joffe, K. Kieburtz, R. Raman, X. Sun, P.S. Aisen, E. Siemers, H. Liu-Seifert, R. Mohs, Alzheimer's disease cooperative study steering committee, Solanezumab Study Group, Phase 3 trials of solanezumab for mild–to–moderate Alzheimer's disease, N. Eng. J. Med. 370 (2014) 311–321.
[17] (a) L. Lannfelt, K. Blennow, H. Zetterberg, S. Batsman, D. Ames, J. Harrison, C.L. Masters, S. Targum, A.I. Bush, R. Murdoch, J. Wilson, C.W. Ritchie, PBT2–201–EURO study group, Safety, efficacy, and biomarker findings of PBT2 in targeting Aβ as a modifying therapy for Alzheimer's disease: a phase IIa, double––blind, randomised, placebo–controlled trial, Lancet Neurol. 7 (2008) 779–786; (b) C.W. Ritchie, A.I. Bush, A. Mackinnon, S. Macfarlane, M. Mastwyk, L. MacGregor, L. Kiers, R. Cherny, Q.X. Li, A. Tammer, D. Carrington, C. Mavros, I. Volitakis, M. Xilinas, D. Ames, S. Davis, K. Beyreuther, R.E. Tanzi, C.L. Masters, Metal–protein attenuation with iodochlorhydroxyquin (clioquinol) targeting Abeta

amyloid deposition and toxicity in Alzheimer disease: a pilot phase 2 clinical trial, Arch. Neurol. 60 (2003) 1685–1691.

[18] (a) Q. Li, S. He, Y. Chen, F. Feng, W. Qu, H. Sun, Donepezil-based multi-functional cholinesterase inhibitors for treatment of Alzheimer's disease, Eur. J. Med. Chem. 158 (2018) 463–477;
(b) D. Knez, N. Coquelle, A. Pišlar, S. Žakelj, M. Jukič, M. Sova, J. Mravljak, F. Nachon, X. Brazzolotto, J. Kos, J.-P. Colletier, S. Gobec, Multi-target-directed ligands for treating Alzheimer's disease: Butyrylcholinesterase inhibitors displaying antioxidant and neuroprotective activities, Eur. J. Med. Chem. 156 (2018) 598–617;
(c) M.G. Savelieff, G. Nam, J. Kang, H.J. Lee, M. Lee, M.H. Lim, Development of multifunctional molecules as potential therapeutic candidates for Alzheimer's disease, Parkinson's disease, and amyotrophic lateral sclerosis in the last decade, Chem. Rev. 119 (2019) 1221–1322;
(d) X. Zhang, K.P. Rakesh, S.N.A. Bukhari, M. Balakrishna, H.M. Manukumar, H.L. Qin, Multi-targetable chalcone analogs to treat deadly Alzheimer's disease: current view and upcoming advice, Bioorg. Chem. 80 (2018) 86–93;
(e) S. Das, S. Basu, Multi–targeting strategies for Alzheimer's disease therapeutics: pros and cons, Curr. Top. Med. Chem. 17 (2017) 3017–3061;
(f) H. Lin, Q. Li, K. Gu, J. Zhu, X. Jiang, Y. Chen, H. Sun, Therapeutic agents in Alzheimer's disease through a multi–target directed ligands strategy: recent progress based on tacrine core, Curr. Top. Med. Chem. 17 (2017) 3000–3016;
(g) K. Spilovska, J. Korabecny, E. Nepovimova, R. Dolezal, E. Mezeiova, O. Soukup, K. Kuca, Multitarget tacrine hybrids with neuroprotective properties to confront Alzheimer's disease, Curr. Top. Med. Chem. 17 (2017) 1006–1026;
(h) X.T. Luo, C.M. Wang, Y. Liu, Z.G. Huang, New multifunctional melatonin–derived benzylpyridinium bromides with potent cholinergic, antioxidant, and neuroprotective properties as innovative drugs for Alzheimer's disease, Eur. J. Med. Chem. (2015) 302–311;
(i) Z. Wang, Y. Wang, B. Wang, W. Li, L. Huang, X. Li, Design, synthesis, and evaluation of orally available clioquinol–moracin M hybrids as multitarget–directed ligands for cognitive improvement in a rat model of neurodegeneration in Alzheimer's disease, J. Med. Chem. 58 (2015) 8616–8637.

[19] (a) R. Pouplana, J.M. Campanera, Energetic contributions of residues to the formation of early amyloid–β oligomers, Phys. Chem. Chem. Phys. 17 (2015) 2823–2837;
(b) B. Chandra, S. Halder, J. Adler, A. Korn, D. Huster, S. Maiti, Emerging structural details of transient amyloid–β oligomers suggest designs for effective small molecule modulators, Chem. Phys. Lett. 675 (2017) 51–55.

[20] J. Hardy, Has the amyloid cascade hypothesis for Alzheimer's disease been proved? Curr. Alzheimer Res. 3 (2006) 71–73.

[21] (a) D. Goyal, S. Shuaib, S. Mann, B. Goyal, Rationally designed peptides and peptidomimetics as inhibitors of amyloid–β (Aβ) aggregation: potential therapeutics of Alzheimer's disease, ACS Comb. Sci. 19 (2017) 55–80;
(b) S.A. Funke, D. Willbold, Peptides for therapy and diagnosis of Alzheimer's disease, Curr. Pharm. Des. 18 (2012) 755–767;
(c) J. Kumar, V. Sim, D–amino acid–based peptide inhibitors as early or preventative therapy in Alzheimer disease, Prion 8 (2014) 119–124;
(d) A. Francioso, P. Punzi, A. Boffi, C. Lori, S. Martire, C. Giordano, M. D'Erme, L. Mosca, β–sheet interfering molecules acting against β–amyloid aggregation and fibrillogenesis, Biorg. Med. Chem. 23 (2015) 1671–1683;
(e) H. Li, F. Rahimi, G. Bitan, Modulation of amyloid β–Protein (Aβ) assembly by homologous C–terminal fragments as a strategy for inhibiting Aβ toxicity, ACS Chem. Neurosci. 7 (2016) 845–856;
(f) A.J. Doig, P. Derreumaux, Inhibition of protein aggregation and amyloid formation by small molecules, Curr. Opin. Struct. Biol. 30 (2015) 50–56;
(g) F. Belluti, A. Rampa, S. Gobbi, A. Bisi, Small–molecule inhibitors/modulators of amyloid–β peptide aggregation and toxicity for the treatment of Alzheimer's disease: a patent review (2010–2012), Expert Opin. Ther. Pat. 23 (2013) 581–596;
(h) Z. Liu, A. Zhang, H. Sun, Y. Han, L. Kong, X. Wang, Two decades of new drug discovery and development for Alzheimer's disease, RSC Adv. 7 (2017) 6046–6058.

[22] (a) J. Dong, C.S. Atwood, V.E. Anderson, S.L. Siedlak, M.A. Smith, G. Perry, P.R. Carey, Metal binding and oxidation of amyloid–β within isolated senile plaque cores: Raman microscopic evidence, Biochemistry 42 (2003) 2768–2773;
(b) K.P. Kepp, Bioinorganic chemistry of Alzheimer's disease, Chem. Rev. 112 (2012) 5193–5239.

[23] T.A. Bayer, S. Schäfer, A. Simons, A. Kemmling, T. Kamer, R. Tepest, A. Eckert, K. Schüssel, O. Eikenberg, C. Sturchler-Pierrat, D. Abramowski, M. Staufenbiel, G. Multhaup, Dietary Cu stabilizes brain superoxide dismutase 1 activity and reduces amyloid Aβ production in APP23 transgenic mice, Proc. Natl. Acad. Sci. USA 100 (2003) 14187–14192.

[24] W. Huang, W. Wei, Z. Shen, Drug–like chelating agents: a potential lead for Alzheimer's disease, RSC Adv. 4 (2014) 52088–52099.

[25] K.J. Barnham, C.L. Masters, A.I. Bush, Neurodegenerative diseases and oxidative stress, Nat. Rev. Drug Discov. 3 (2004) 205–214.

[26] (a) C. Lu, Y. Guo, J. Yan, Z. Luo, H.-B. Luo, M. Yan, L. Huang, X. Li, Design, synthesis, and evaluation of multitarget–directed resveratrol derivatives for the treatment of Alzheimer's disease, J. Med. Chem. 56 (2013) 5843–5859;
(b) L. Huang, C. Lu, Y. Sun, F. Mao, Z. Luo, T. Su, H. Jiang, W. Shan, X. Li, Multitarget–directed benzylideneindanone derivatives: anti–β–amyloid (Aβ) aggregation, antioxidant, metal chelation, and monoamine oxidase B (MAO–B) inhibition properties against Alzheimer's disease, J. Med. Chem. 55 (2012) 8483–8492.

[27] (a) D. Goyal, A. Kaur, B. Goyal, Benzofuran and indole: promising scaffolds for drug development in Alzheimer's disease, ChemMedChem 13 (2018) 1275–1299;
(b) D. Dheer, V. Singh, R. Shankar, Medicinal attributes of 1,2,3-triazoles: Current developments, Bioorg. Chem. 71 (2017) 30–54;
(c) H. Kroth, C. Hamel, P. Benderitter, W. Froestl, N. Sreenivasachary, A. Muhs, Ac Immune S.A., Preparation of 7–azaindole, indole, and carbazole compounds for the treatment of diseases associated with amyloid or amyloid–like proteins patent. WO2011128455A1, 2011.
(d) P. Thirumurugan, D. Matosiuk, K. Jozwiak, Click chemistry for drug development and diverse chemical – biology applications, Chem. Rev. 113 (2013) 4905–4979

[28] W. Qu, M.P. Kung, C. Hou, S. Oya, H.F. Kung, Quick assembly of 1,4–diphenyltriazoles as probes targeting beta–amyloid aggregates in Alzheimer's disease, J. Med. Chem. 50 (2007) 3380–3387.

[29] S. Das, S.D. Smid, Identification of dibenzylimidazolidine and triazole acetamide derivatives through virtual screening targeting amyloid beta aggregation and neurotoxicity in PC12 cells, Eur. J. Med. Chem. 130 (2017) 354–364.

[30] K. Arunrungvichian, V.V. Fokin, O. Vajragupta, P. Taylor, Selectivity optimization of substituted 1,2,3–triazoles as α7 nicotinic acetylcholine receptor agonists, ACS Chem. Neurosci. 6 (2015) 1317–1330.

[31] M.R. Jones, E. Mathieu, C. Dyrager, S. Faissner, Z. Vaillancourt, K.J. Korshavn, M.H. Lim, A. Ramamoorthy, V.W. Yong, S. Tsutsui, P.K. Stys, T. Storr, Multi–target–directed phenol–triazole ligands as therapeutic agents for Alzheimer's disease, Chem. Sci. 8 (2017) 5636–5643.

[32] J. Jiaranaikulwanitch, P. Govitrapong, V.V. Fokin, O. Vajragupta, From BACE1 inhibitor to multifunctionality of tryptoline and tryptamine triazole derivatives for Alzheimer's disease, Molecules 17 (2012) 8312–8333.

[33] A.S. Reddy, S. Zhang, Polypharmacology: drug discovery for the future, Expert Rev. Clin. Pharmacol. 6 (2013) 41–47.

[34] (a) D. Ghosh, S. Rhodes, D. Winder, A. Atkinson, J. Gibson, W. Ming, C. Padgett, S. Landge, K. Aiken, Spectroscopic investigation of bis–appended 1,2,3–triazole probe for the detection of Cu(II) ion, J. Mol. Struct. 1134 (2017) 638–648;
(b) S. Kotha, D. Goyal, S. Banerjee, A. Dutta, A novel di–triazole based peptide as a highly sensitive and selective fluorescent chemosensor for Zn2+ ions, Analyst 137 (2012) 2871–2875.

[35] (a) H.C. Kolb, M.G. Finn, K.B. Sharpless, Click chemistry: diverse chemical function from a few good reactions, Angew. Chem. Int. Ed. 40 (2001) 2004–2021;
(b) V.V. Rostovtsev, L.G. Green, V.V. Fokin, K.B. Sharpless, A stepwise Huisgen cycloaddition process: copper(I)–catalyzed regioselective "ligation" of azides and terminal alkynes, Angew. Chem. Int. Ed. Engl. 41 (2002) 2596–2599.

[36] S. Kotha, K. Mohanraja, S. Durani, Constrained phenylalanyl peptides via a [2+2+2]–cycloaddition strategy, Chem. Commun. (2000) 1909–1910.

[37] C. Gill, G. Jadhav, M. Shaikh, R. Kale, A. Ghawalkar, D. Nagargoje, M. Shiradkar, Clubbed [1,2,3] triazoles by fluorine benzimidazole: a novel approach to H37Rv inhibitors as a potential treatment for tuberculosis, Bioorg. Med. Chem. Lett. 18 (2008) 6244–6247.

[38] H. LeVine, Thioflavine T interaction with amyloid β–sheet structures, Amyloid 2 (1995) 1–6.

[39] F. Yang, G.P. Lim, A.N. Begum, O.J. Ubeda, M.R. Simmons, S.S. Ambegaokar, P.P. Chen, R. Kayed, C.G. Glabe, S.A. Frautschy, G.M. Cole, Curcumin inhibits formation of amyloid beta oligomers and fibrils, binds plaques, and reduces amyloid in vivo, J. Biol. Chem. 280 (2005) 5892–5901.

[40] (a) E.P. Vieira, H. Hermel, H. Möhwald, Change and stabilization of the amyloid–beta (1–40) secondary structure by fluorocompounds, Biochim. Biophys. Acta. 1645 (2003) 6–14;
(b) A. Rahman, M.T. Ali, M.M. Shawan, M.G. Sarwar, M.A. Khan, M.A. Halim, Halogen–directed drug design for Alzheimer's disease: a combined density functional and molecular docking study, Springerplus 5 (2016) 1346;
(c) M. Török, M. Abid, S.C. Mhadgut, B. Török, Organofluorine inhibitors of amyloid fibrillogenesis, Biochemistry 45 (2006) 5377–5383.

[41] S.S. Hindo, A.M. Mancino, J.J. Braymer, Y. Liu, S. Vivekanandan, A. Ramamoorthy, M.H. Lim, Small molecule modulators of copper–induced Aβ aggregation, J. Am. Chem. Soc. 131 (2009) 16663–16665.

[42] L. Guilloreau, S. Combalbert, A. Sournia-Saquet, H. Mazarguil, P. Faller, Redox chemistry of copper–amyloid–beta: the generation of hydroxyl radical in the presence of ascorbate is linked to redox–potentials and aggregation state, ChemBioChem 8 (2007) 1317–1325.

[43] F. Mao, J. Yan, J. Li, X. Jia, H. Miao, Y. Sun, L. Huang, X. Li, New multi–target–directed small molecules against Alzheimer's disease: a combination of resveratrol and clioquinol, Org. Biomol. Chem. 12 (2014) 5936–5944.

[44] Z. Wang, S. Tao, X. Dong, Y. Sun, Para–sulfonato–calix[n]arenes inhibit amyloid beta–peptide fibrillation and reduce amyloid cytotoxicity, Chem. Asian J. 12 (2017) 341–346.

[45] J.T. Jarrett, E.P. Berger, P.T. Lansbury Jr, The carboxy terminus of the amyloid protein is critical for the seeding of amyloid formation: implications for the pathogenesis of Alzheimer's disease? Biochemistry 32 (1993) 4693–4697.

[46] G.M. Morris, D.S. Goodsell, R.S. Halliday, R. Huey, W.E. Hart, R.K. Belew, A.J. Olson, Automated docking using a Lamarckian genetic algorithm and an empirical binding free energy function, J. Comput. Chem. 19 (1998) 1639–1662.

[47] (a) F.J. Solis, R.J.–B. Wets, Minimization by random search techniques, Math. Meth. Oper. Res. 6 (1981) 19–30;
(b) R. Huey, G.M. Morris, A.J. Olson, D.S. Goodsell, A semiempirical free energy force field with charge–based desolvation, J. Comput. Chem. 28 (2007) 1145–1152.